



**Πανεπιστήμιο Αιγαίου**  
Τμήμα Μηχανικών Πληροφοριακών & Επικοινωνιακών Συστημάτων

---

# Αναγνώριση Γραφεία

---

Παρασκευάς Διαμαντάτος

**Επιβλέπων: Αναπληρώτρια Καθηγήτρια: Εργίνα Καβαλλιεράτου**

Καρλόβασσι – Σάμος - Ελλάδα 20/09/2021

---

Διατριβή  
για την απόκτηση Διδακτορικού Διπλώματος του  
Εργαστηρίου Τεχνητής Νοημοσύνης & Συστημάτων Στήριξης Αποφάσεων του  
Τμήματος Μηχανικών Πληροφοριακών και Επικοινωνιακών Συστημάτων

---



**UNIVERSITY OF THE AEGEAN**  
Department of Information and Communication Systems Engineering

---

## **WRITER IDENTIFICATION**

---

**Ph.D. Dissertation**  
**Paraskevas Diamantatos**

**Supervisor: Associate Professor: Ergina Kavallieratou**

Karlovassi – Samos – Greece 20/09/2021

---

Submitted in Total Fulfilment  
of the Requirements for  
The degree of Doctor of Philosophy (PhD)

---

## Declaration of Authorship

I, Paraskevas Diamantatos, declare that this Dissertation entitled “Writer Identification” and all the work presented here is my own and has been generated as the result of my original research. I confirm that:

- This work was done wholly while in candidature for a research degree at this University.
- It is always clearly attributed where I have consulted the published work of others.
- The source is always given, where I have quoted from the work of others. Except for such quotations, this thesis is entirely my work.
- I have acknowledged all the sources of help.
- The thesis is based on work done by myself jointly with others. I have made it clear precisely what was done by others and what I have contributed myself.

Signed:

---

Date:

---

# Advising Committee

---

Associate Professor  
Ergina Kavallieratou

---

---

Professor  
Efstathios Stamatatos

---

---

Professor  
Manolis Maragoudakis

---

# Examining Committee

---

Associate Professor : Kavallieratou Ergina

---

---

Professor : Efstathios Stamatatos

---

---

Professor : Manolis Maragoudakis

---

---

Professor : Stefanos Gritzalis

---

---

Professor : Athanassios Skodras

---

---

Professor : Ioannis Pratikakis

---

---

Associate Professor : Theodoros Kostoulas

---

# Abstract

The state-of-the-art writer identification systems use various features and techniques to identify the writer of the handwritten text. In this work, several directional features and combinations of directional with model-based features are presented. Specifically, several improvements of a statistical, directional feature, the edge hinge distribution, are attempted in novel contributions as the Skeleton Hinge Distribution, the Weighted Skeleton Hinge Distribution, the Quantized Skeleton Hinge Distribution, the Directional Stroke Run Length Distribution and the Edge Skeleton Hinge combination. Furthermore, the Skeleton Hinge Distribution feature with a model-based feature is explored, based on a codebook of graphemes.

Novel contributions related to the preprocessing of the document images and the extraction of valuable characteristics are presented. More specifically, two techniques are presented for Main Body Size estimation, a characteristic with application in a broad range of document image analysis fields. One measures Main Body size directly, while the other does an estimation for the baselines first. Both methods are segmentation free. A collection of 10 printed document images and a collection of handwritten text were used for the presented experimental results.

Furthermore, a technique for text localization is presented that takes advantage of the fact that text should present some contrast in comparison with the background, to be distinguished by the human eye. A procedure of binarization is applied to create appropriate images for text detection. The connected components of the image are extracted, and some heuristic rules are applied to identify areas containing text.

For the evaluation, the Firemaker Database and the ICDAR 2017 writer identification competition dataset were used. A plethora of matching techniques were considered for Skeleton Hinge distribution, including nearest neighbour classifier, K-means, Hierarchical Cluster Tree, k-nearest neighbours and Support Vector Machines. The skeleton hinge distribution achieved an accuracy of 90,8%, while the combination of this method with the codebook of graphemes reached 96%. The Weighted Skeleton Hinge Distribution achieved an accuracy of 91.2%. The Quantized Skeleton Hinge Distribution achieved an accuracy of 92.4%. The Directional Stroke Run Length Distribution achieved an accuracy of 91.2%, and finally, the Edge Skeleton Hinge combination technique achieved an accuracy of 90,2%.

Keywords: Writer Identification, Edge-Hinge Distribution, Skeleton-Hinge Distribution, Codebook of Graphemes

# Περίληψη

Τα σύγχρονα συστήματα αναγνώρισης γραφέα χρησιμοποιούν μια ποικιλία διαφορετικών χαρακτηριστικών και τεχνικών για να προσδιορίσουν τον συγγραφέα του χειρόγραφου κειμένου. Σε αυτή την διατριβή παρουσιάζονται διάφορα κατευθυντικά χαρακτηριστικά καθώς και συνδυασμοί κατευθυντικών χαρακτηριστικών με χαρακτηριστικά που βασίζονται σε μοντέλα. Συγκεκριμένα, επιχειρούνται αρκετές βελτιώσεις ενός στατιστικού, κατευθυντικού χαρακτηριστικού, του edge hinge distribution. Τα νέα χαρακτηριστικά που παρουσιάζονται είναι το Skeleton Hinge Distribution, το Weighted Skeleton Hinge Distribution, το Quantized Skeleton Hinge Distribution, το Directional Stroke Run Length Distribution και το Edge Skeleton Hinge Combination . Επιπλέον, διερευνάται ο συνδυασμός του Skeleton Hinge Distribution με ένα χαρακτηριστικό που βασίζεται σε μοντέλα.

Νέες συνεισφορές που σχετίζονται με την προεπεξεργασία των εικόνων εγγράφων αλλά και την εξαγωγή πολύτιμων χαρακτηριστικών του κειμένου. Ειδικότερα, παρουσιάζονται δύο τεχνικές για την εκτίμηση μεγέθους κύριου σώματος (Main Body Size Estimation), το οποίο είναι ένα χαρακτηριστικό του κειμένου με εφαρμογή σε ένα ευρύ φάσμα πεδίων ανάλυσης εικόνων εγγράφου. Η πρώτη μέθοδος μετρά άμεσα το μέγεθος του κύριου σώματος, ενώ η δεύτερη υπολογίζει πρώτα τις βασικές γραμμές (baseline). Και οι δύο προτινόμενοι μέθοδοι δεν απαιτούν τμηματοποίηση (segmentation) . Τα πειραματικά αποτελέσματα παρουσιάζονται σε μια συλλογή χειρόγραφων εγγράφων καθώς και σε μια μικρή συλλογή 10 εικόνων απο πληκτρολογημένα εγγράφα προκειμένου να προκύψουν πιο αντικειμενικά αποτελέσματα. Επιπλέον, παρουσιάζετε μια τεχνική για τον εντοπισμό κειμένου που εκμεταλλεύεται το γεγονός ότι το κείμενο πρέπει να παρουσιάζει κάποια αντίθεση σε σχέση με το υπόβαθρο (background), προκειμένου να διακρίνεται από το ανθρώπινο μάτι. Χρησιμοποιείται μια διαδικασία binarization για τη δημιουργία κατάλληλων εικόνων εγγράφου για την ανίχνευση κειμένου. Στην συνέχεια τα συνδεδεμένα στοιχεία (connected components) της εικόνας εξάγονται και εφαρμόζονται ορισμένοι ευρετικοί κανόνες για τον εντοπισμό περιοχών που περιέχουν κείμενο.

Για την αξιολόγηση της παρούσας εργασίας, η συλλογή χειρόγραφων firmaker DB χρησιμοποιήθηκε. Η συγκεκριμένη συλλογή περιλαμβάνει 4 σελίδες χειρόγραφου κειμένου από 250 διαφορετικούς συγγραφείς. Χρησιμοποιήθηκε μια πληθώρα τεχνικών αντιστοίχισης για το Skeleton Hinge Distribution, συμπεριλαμβανομένου του πλησιέστερου γείτονα, k-means, ιεραρχικών συστάδων (hierarchical cluster trees) , knn και support vector machines. Το χαρακτηριστικό Skeleton Hinge Distribution κατάφερε να ανιχνεύσει τον συγγραφέα χειρόγραφου κειμένου με ακρίβεια 90,8%, το Weighted Skeleton Hinge Distribution με ακρίβεια 91,2%, το Quantized Skeleton Hinge Distribution με ακρίβεια 92,4%, το Directional Stroke Run Length Distribution με ακρίβεια 91,2% και το Edge Skeleton Hinge Combination με ακρίβεια 90,2%.





«Make everything as simple as  
possible, but not simpler.»

Albert Einstein

## **Acknowledgements**

I want to thank my PhD Supervisor Ergina Kavallieratou for her support and guidance. The advising and examining committee for their time, effort and support. Professor Stefanos Gritzalis for his support and understanding during the period of my PhD.

I am incredibly grateful to all my colleagues and friends for the nice times we had together during the period of my PhD.

I would also like to thank my girlfriend Klelia. She encouraged me in difficult times and never stopped believing in me.

Most importantly, I want to thank my Family for their support in my entire student's life. Without their help, this PhD Dissertation would not be possible.

## List of Publications

- Diamantatos, P., Kavallieratou, E., & Gritzalis, S. (2021). Directional Hinge Features for Writer Identification: The importance of the Skeleton and the effects of character size and pixel intensity. *SN Computer Science* – Under Review - Second Revision
- Diamantatos, P., Kavallieratou, E., & Gritzalis, S. (2016). Skeleton Hinge Distribution for Writer Identification. *International Journal on Artificial Intelligence Tools*, 25(03), 1650015.
- Diamantatos, P., Stefanos, G., & Ergina, K. (2014, September). Writer identification using a statistical and model based approach. In *2014 14th International Conference on Frontiers in Handwriting Recognition* (pp. 589-594). IEEE.
- Diamantatos, P., Kavallieratou, E., & Gomez-Gil, P. (2014, September). Binarization: a Tool for Text Localization. In *2014 14th International Conference on Frontiers in Handwriting Recognition* (pp. 649-654). IEEE.
- Diamantatos, P., Verras, V., & Kavallieratou, E. (2013, August). Detecting main body size in document images. In *2013 12th International Conference on Document Analysis and Recognition* (pp. 1160-1164). IEEE.
- Diamantatos, P., & Kavallieratou, E. (2014, September). Android based electronic travel aid system for blind people. In *IFIP International Conference on Artificial Intelligence Applications and Innovations* (pp. 585-592). Springer, Berlin, Heidelberg.

# Contents

Declaration of Authorship .....	3
Advising Committee.....	4
Examining Committee.....	5
Abstract.....	6
Περίληψη.....	7
Acknowledgements .....	10
List of Publications.....	11
Contents.....	12
List of Figures.....	15
List of Tables.....	18
1. Writer Identification.....	19
1.1 Introduction.....	19
1.2 Motivation And Objectives.....	21
1.3 Main Assumptions .....	22
1.4 Contributions .....	22
1.5 Overview.....	23
2. State Of The Art.....	24
3. Handwritten Document Image.....	28
3.1 Handwritten Document Image Anatomy .....	28
3.2 Terms Definition.....	30
3.3 Document Image Analysis.....	31
3.3.1 Digital Image.....	31
3.3.2 Binarization .....	32
3.3.3 Edge Detection .....	33
3.3.4 Gabor Filter .....	34
3.3.5 Skeletonization .....	34
3.3.6 Connected Components.....	35
3.3.7 Contour Tracing.....	35
3.3.8 Main Body.....	36
3.3.9 Run Length Encoding.....	37
3.3.10 Fourier Transformation .....	37
3.3.11 Text Localization.....	38
4. Writer Identification Techniques .....	39

4.1	Statistical-Directional Features .....	39
4.1.1	Edge-Direction Distribution .....	39
4.1.2	Edge-Hinge Distribution .....	40
4.1.3	Edge-Hinge Combinations .....	41
4.1.4	Skeleton-Hinge Distribution.....	41
4.1.5	Weighted Skeleton-Hinge Distribution .....	47
4.1.5.1	Main Body Size And Main Body Map.....	48
4.1.5.2	Main Body Size Extraction And Weighted Skeleton Hinge .....	49
4.1.6	Quantized Skeleton Hinge Distribution.....	51
4.1.7	Directional Stroke Run Length Hinge Distribution.....	52
4.1.8	Run Length Directional Skeleton Hinge Distribution .....	55
4.1.9	Edge-Skeleton-Hinge Combinations .....	55
4.2	Model-Based Features .....	57
5.	Main Body And Text Localization .....	59
5.1	Introduction.....	59
5.2	Main Body Size Estimation .....	59
5.2.1	First Technique .....	59
5.2.2	Second Technique .....	61
5.2.3	Experimental Results.....	64
5.3	Text Localization .....	66
5.3.1	System Overview.....	66
5.3.2	Experimental Results.....	69
6.	Writer Identification Experimental Results .....	70
6.1	Data Sets .....	70
6.1.1	Firemaker DB .....	70
6.1.2	ICDAR 2017 Writer Identification Competition.....	70
6.2	Experiments .....	71
6.2.1	Skeleton Hinge Distribution .....	71
6.2.1.1	Skeleton Hinge Features With The Nearest Neighbour Classifier On Firemaker DB.....	71
6.2.1.2	Skeleton Hinge Features With The Nearest Neighbour Classifier On ICDAR 201772	
6.2.1.3	Skeleton Hinge Features With K-means And Hierarchical Cluster Tree Identification Results.....	73
6.2.1.4	Skeleton Hinge Features With Nearest Neighbor Using KNN Results. ..	74

6.2.1.5 Skeleton Hinge Features With Support Vector Machines Results.....	75
6.2.2 Codebook of Graphemes And Skeleton Hinge Distribution .....	75
6.2.3 Quantized Skeleton Hinge Distribution.....	76
6.2.4 Weighted Skeleton Hinge.....	76
6.2.5 Run Length Directional Hinge .....	77
6.2.6 Edge Skeleton Hinge Combination .....	78
6.2.7 Directional Features Comparison .....	78
6.2.8 Filtering With Text Localization Method.....	80
6.2.9 ICDAR 2017 Experiments .....	81
7. Discussions And Conclusion .....	83
7.1 Directional Hinge Features Interpretation .....	83
7.2 Discussions .....	87
7.3 Conclusion .....	88
References .....	90

# List of Figures

Figure 1. Example of a part of a handwritten historical document image from the ICDAR 2013 Handwriting Segmentation Contest [55] benchmark dataset with interfering lines (ellipse), non-uniform skew, non-uniform interlines spacing and text lines with curvature. .... 28

Figure 2. Example of a part of a handwritten historical document image from the ICDAR 2013 Handwriting Segmentation Contest benchmark dataset with connected lines (circles), non-uniform skew and non-uniform interline spacing (line). .... 28

Figure 3. Example of handwritten historical document images from the ICDAR 2013 Handwriting Segmentation Contest benchmark dataset, scaled to 5% of the original size. Text lines can be distinguished from a human, even on this scale. .... 29

Figure 4. Example of handwritten historical document images from the ICDAR 2013 Handwriting Segmentation Contest [10] benchmark dataset, scaled to 5% of the original size. Text lines can be distinguished from a human, even on this scale. .... 29

Figure 5. Upper line, Median line, Baseline, Lower line, a single stroke, ascenders and descenders. .... 30

Figure 6. Square: touching components. Circle: overlapping components. .... 31

Figure 7. Fragment of a digital image with the word “The” ..... 31

Figure 8. Fragment of a digital image with the character “e”, zoomed to the pixel level.. 32

Figure 9. the character “e” represented in a pixel intensity matrix ..... 32

Figure 10. The character "e" is represented in a binary pixel intensity matrix ..... 33

Figure 11. The output of edge detection on the image of Fig. 7. .... 33

Figure 12. Top left: Original Chinese character. Top middle: Orientation = 0 degree. Top right: Orientation = 45 degree. Bottom middle: Orientation = 90 degree. Bottom right: Orientation = 135 degree. Bottom left: Superposition of all four orientations. .... 34

Figure 13. The output of skeletonization on the image of Fig. 7. .... 35

Figure 14. left: 8-connectivity. Also called a Moore neighbourhood. right: 4-connectivity ..... 35

---

Figure 15. left: The character “A”. right: The complete contour of character “A”. .... 36

Figure 16. Word Main Body and baselines. .... 36

Figure 17. An example of a pixel sequence with a black run length with values 2, 3, 7, 2, 3 ..... 37

---

Figure 18. Handwritten characters, along with their Magnitude in the Fourier domain ... 38

Figure 19. Extraction of edge-direction distribution. .... 40

Figure 20. Edge Hinge Distribution Extraction..... 41

Figure 21. Handwritten digitized text..... 42

Figure 22. Edge image of handwritten text ..... 42

Figure 23. Skeleton image of handwritten text ..... 43

Figure 24. 4 pixels long Hinge line fragments, emerging from a central pixel, on a 7x7 window..... 43

Figure 25. An instance of Skeleton Hinge distribution extraction with four pixels-long edge fragments on the part of the word “Bob”..... 44

Figure 26. Text samples from the same writer along with skeleton hinge distribution feature surface (middle) and edge hinge combinations feature surface (bottom)..... 45

Figure 27. Text samples from the same writer along with skeleton hinge distribution feature surface (middle) and edge hinge combinations feature surface (bottom)..... 46

Figure 28. Text samples from the same writer along with skeleton hinge distribution feature surface (middle) and edge hinge combinations feature surface (bottom).....	47
Figure 29. Word main body and baselines .....	48
Figure 30. Main Body Map Example .....	48
Figure 31. Main Body Map projected on the document image .....	49
Figure 32. Handwritten document image with a resolution of 1232x2076 .....	50
Figure 33. The smoothed version of the document image with the parameter C set to 60 pixels and resolution 1232x34 .....	50
Figure 34. Example of the letter O .....	50
Figure 35. Example of the corresponding smoothed image of the letter O with a height of 35 pixels and width of 1.....	51
Figure 36. Bimodal distribution .....	51
Figure 37. An instance of Stroke Run Length Directional Hinge window of 6 pixels-long fragments with the central pixel selected as starting point. ....	52
Figure 38. cardinal and intermediate directions will be used to describe run-length directions .....	53
Figure 39. The selected Starting point along with the run lengths in 8 directions with the largest one being 6 pixels length with North direction and the second largest with 5 pixels length on South-East direction.....	53
Figure 40. The five directions emerging from the second point along with the run lengths in five directions, with the largest one being in the North-East direction .....	53
Figure 41. The Largest Run Length is followed until the border is reached.....	53
Figure 42. The next pixel is selected in the direction of the second largest direction.....	54
Figure 43. The five directions emerging from the first point on the second-largest direction along with the run lengths in five directions, with the largest one being in the East direction ....	54
Figure 44. The five directions are emerging from the second point on the second-largest direction and the run lengths in five directions with two directions of equal length of four pixels. The East direction is selected since it was also the direction selected in the previous step. ....	54
Figure 45. The five directions emerging from the third point on the second-largest direction along with the run lengths in five directions, with the largest one being in the South East direction .....	54
Figure 46. The Largest Run Length is followed until the border is reached.....	55
Figure 47. Final Stroke Run Length Directional Hinge with six pixels-long fragments ...	55
Figure 48. Skeleton-Hinge feature with the area denoted with the triangle being empty ..	56
Figure 49. Feature spaces from the Edge-Skeleton Hinge Combinations on the Test sample .....	56
Figure 50. Feature spaces from the Edge-Skeleton Hinge Combinations on Train sample from the same writer. ....	57
Figure 51. Writers attempt to erase with ink what he has written by mistake .....	59
Figure 52. The proposed Main Body Size Extraction methodology. ....	60
Figure 53. Schematic presentation of the technique through example.....	61
Figure 54. Vertical dilate.....	62
Figure 55. Vertical text localization. ....	62
Figure 56. The second technique.....	63
Figure 57. Horizontal dilate.....	63
Figure 58. Horizontal text localization.....	64



Figure 59. Result with upper and lower baselines visible .....	64
Figure 60. The tasks of the proposed system .....	67
Figure 61. Text localization result example of the document from Figure 51. ....	68
Figure 62. Final image after text localization, on the document from Figure 51. ....	69
Figure 63. Part of a Document image from Firemaker DB.....	70
Figure 64. EHC, SHD, WSHD, RLDHD identification accuracy on Firemaker DB.....	80
Figure 65. An example of different Slant Angles from left to right. The graphic is from [103]......	83
Figure 66. An example of right slanted (a), left slanted (b) and variant slanted(c) word. The graphic is from [104]. .....	84
Figure 67. Part of text from Firemaker DataSet from writer 1657.....	84
Figure 68 Polar plot of the angles $\phi_1$ , $\phi_2$ and their difference $\phi_2-\phi_1$ for writer 1657 .....	84
Figure 69 Part of text from Firemaker DataSet from writer 17.....	85
Figure 70 Polar plot of the angles $\phi_1$ , $\phi_2$ and their difference $\phi_2-\phi_1$ for writer 17 .....	85
Figure 71 Train and Test samples from writer 52 of Firemaker Dataset .....	86
Figure 72 Train and Test samples from writer 23 of Firemaker Dataset .....	86
Figure 73 with solid lines writer 52 from train dataset and dashed line writer 23 from the test dataset. ....	86
Figure 74 writer 52 differences between train and test dataset .....	87
Figure 75 Same words from writer 52 and 23 from Firemaker data set.....	87

## List of Tables

Table 1.	Examples of Main Body size estimation .....	65
Table 2.	Experimental Results .....	65
Table 3.	Comparative results with the dataset of ICDAR 2011 Robust Reading Competition Challenge 2: Reading Text in Scene Images [96].....	69
Table 4.	Skeleton Hinge Distribution Accuracy (Percentage) on Firemaker DB.....	72
Table 5.	Skeleton Hinge Distribution Accuracy (Percentage) on ICDAR 2017 writer identification competition Data Set .....	73
Table 6.	Skeleton Hinge Distribution Accuracy (Percentage) on ICDAR 2017 writer identification competition Data Set as reported in [15].....	73
Table 7.	K-means and Hierarchical cluster tree identification Results on Firemaker DB	74
Table 8.	Skeleton Hinge Identification Accuracy using KNN on Firemaker DB.....	74
Table 9.	Skeleton Hinge Features with Support Vector Machines results on Firemaker DB.	75
Table 10.	Skeleton Hinge Distribution Combined with Codebook of Graphemes Method Accuracy (Percentage) on Firemaker DB.....	76
Table 11.	Quantized Skeleton Hinge Distribution Accuracy (Percentage) on Firemaker DB	76
Table 12.	EHC, SHD, WSHD identification Accuracy (Percentage) with Manhattan Distance on Firemaker DB.....	77
Table 13.	EHC, SHD, RLDHD identification Accuracy (Percentage) with Manhattan Distance on Firemaker DB.....	77
Table 14.	EHC, SHD, ESHC identification Accuracy (Percentage) with Manhattan Distance on Firemaker DB.....	78
Table 15.	EDD, EHC, SHD, QSHD, WSHD, RLDHD, ESHC, and methods from literature identification Accuracy (Percentage) with Manhattan Distance on Firemaker DB .....	79
Table 16.	SHD, filtered SHD, ESHC and filtered ESHC identification Accuracy (Percentage) with Manhattan Distance .....	80
Table 17.	SHD, WSHD, RLDSHD, RLDHD, SRLDSHD TOP-1 Identification Accuracy (Percentage) on ICDAR 2017 writer identification competition Data Set.....	81
Table 18.	SHD, WSHD, RLDSHD, RLDHD, 3QSHD MAP Identification Accuracy (Percentage) on ICDAR 2017 writer identification competition Data Set .....	82
Table 19.	Skeleton Hinge Distribution Accuracy (Percentage) on ICDAR 2017 writer identification competition Data Set as reported in [21].....	82

# 1. Writer Identification

## 1.1 Introduction

While our future is digital, our past is analogue. Writing is one of the most important innovations in human history. Our cultural heritage, art, sciences, mythology, religious scripts, poems, certificates, and our entire history can be found in the various historical document collections written over the ages. While these collections are owned by various libraries and private collections worldwide as hard copies, many historical documents have already become digital in the last decades. The digitization of these documents is far from over since more and more collections are digitized every day.

Although the contents of most historical document collections are well known, the same does not apply to the writer identity. Therefore, by developing new methodologies that can identify the writer of a historical document, or retrieve other historical documents from the same writer, or even being able to tell if a historical document is written by one or more writers, like in [1], could allow us to have a better understanding of our history.

Each person's handwriting is unique and therefore it can be used as a biometric characteristic[2]. More specifically, handwriting is considered a behavioural biometric characteristic since it directly relates to how each person grew up. For example, schooling, personal preferences, languages learned, and other characteristics make each writer's handwriting unique. Moreover, handwriting can be affected by other factors like the writing implements used, writing speed, writing surface, and available writing area, resulting in handwritten documents with text characters that may vary in size.

In recent years, most research in person identification primarily targets their biometrics [3]–[5]. Two types of biometrics exist, physiological and behavioural. Physiological biometrics identification applications are based on measuring the physical property of the human body. Various applications offer person identification through their physiological biometrics like their iris, fingerprints, retinal blood vessels, hand geometry, DNA and even face identification from an image. Results that yield a person's identification using physiological biometrics can be considered a solved problem. Behavioural biometrics, on the other hand, uses individual traits of a person's behaviour for identification. Some behavioural biometrics applications include voice identification, signature identification, gait, keystroke dynamics and also handwriting.

Contrary to signature identification[6], which requires a predefined, sort sequence of characters or strokes, writer identification can be achieved by a writer's handwritten text and not only by a predefined one. Moreover, most signature identification systems use online information, meaning that the user signs in a specific area with an electronic pen or some other electronic form of writing aid, which monitors the user's movements and time. Unfortunately, writer identification systems cannot use the same information for practical reasons. Most of the samples are written in the paper, meaning the writer's time to write a text is unknown. Furthermore, the direction he travelled when writing the characters of the text is also unknown.

Writer identification is the task of identifying the writer of an unknown handwritten document image by matching it against a database of handwritten documents with a known writer. First, features are extracted from the handwritten document image, and either a statistical analysis of these features is entailed, and then their distances are measured, or the features are used to construct models, which are later compared, to achieve identification.

In forensic practice, the identification of a writer is a problem that often arises in a court of justice to identify the writer of a handwritten document [7], a will, for example. It also has applications in the health sector where a prescription writer must be verified [8]. While in forensics [9] where writer verification is most common and is usually performed by human experts, writer identification can also be beneficial. For example, in cases of threats, or ransom letters, when there is a suspect for the case, and his handwriting texts are taken as evidence, a graphologist tries to verify the writer's identity with his handwriting texts. The above procedure can be automated if a writer identification system is applied to an extensive data set and output a list of top-ranked writers. Then the results can be either verified by a writer verification system or a human expert. Writer identification and writer verification are some terms that usually get confused [10]. Writer identification systems attempt to match the handwriting of unknown writers against a dataset of handwriting from a known writer. These systems can identify a writer of the handwritten text based on other handwritten text samples from the same writer. Moreover, writer identification systems perform one too many searches in an extensive database with handwriting samples of a known writer and return either one or a list of candidate writers. Writer identification can also be applied to optical character recognition by exploiting the writer's style and adapting the recognition system to the type of the writer [11].

On the other hand, on writer verification systems, the goal is to do a one-to-one identification. Therefore, a decision must be made if two specific handwritten text samples belong to the same writer. In this method, usually, the distance between the two samples is measured, and if it is below a specific threshold, then the two samples are from the same writer.

Writer identification and writer verification fall into two broad categories: text-dependent and text-independent [6]. Text-dependent methods share many similarities with signature verification techniques since they compare a predefined set of characters or words of known semantic meaning with the ones in the handwritten sample in question. Text-dependent methods require human intervention to segment characters or words correctly. On the other hand, text-independent methods use statistical features extracted from the samples without any human intervention. In this work, the main focus will be given in text-independent techniques.

Writer identification techniques can be divided into three broad categories, statistical techniques that use textural [10], [12] or structural based features [13] and model-based approaches that extract features automatically from raw data without explicit programming.

Statistical techniques usually entail a statistical analysis of features extracted from the directionality and curvature or structure of patterns in handwritten document images. In textural features [12], the handwritten document is treated as an image and not as handwriting, and usually, the analysis of the foreground texture is entailed to extract features. In structural features, the extracted features are mainly based on characteristics of the writing that even a human reader can distinguish, such as the text's Main Body size, the height of upper and lower Baselines, character width, and text slant.

Model-based techniques can extract features automatically by using various Artificial-Intelligence techniques like Recurrent Neural Network (RNN), Convolutional Neural Network (CNN), Extend Learning Model (ELM), other deep machine learning models, or allograph approaches [10] that construct models using Self Organizing Feature Maps (SOFM).

This work addresses the problem of offline, text-independent writer identification using scanned handwritten document images. The methods presented here are statistical techniques that capture textural features.

Our methods are statistically evaluated using the Firemaker data set [14] and the ICDAR, 2017 writer identification competition dataset [15].

## 1.2 Motivation And Objectives

The most prominent application of writer identification is in forensics and as evidence in court trials [10]. For example, recently, writer identification techniques [1] were utilized in palaeography to prove that The Great Isaiah Scroll (1QIsaa), one of the original seven Dead Sea Scrolls discovered in Qumran in 1947, was written by two distinct writers carefully mirroring another scribe's writing style. Future advancements in this field may allow us to use it in applications such as OCR, identifying the writer of anonymous historical documents, and authentication systems.

Although relatively recent works on the writer identification field utilize artificial intelligence techniques [15]–[21], a choice was made to use traditional methods only for several reasons.

More specifically, the datasets available for the writer identification task do not contain enough samples and are pretty limited in size. In [17], This issue is identified in the open research issues section as the cause for the scarcity of CNN based writer identification systems in the literature and as a problem that highly affects the performance of deep learning models. Some researchers [21] try to overcome those limitations by using another Artificial Intelligence technique to generate thousands of samples per writer. Other researchers [19], [20] either utilize the annotations available on Datasets to split entire pages into words or proceed with word segmentation techniques and then try to achieve writer identification on the word level.

Moreover, with the recent European Union fit for the Digital Age [22], the EU Commission proposes new rules and actions for excellence and trust in Artificial Intelligence. According to these new rules, biometric identification systems are considered high risk and subject to strict requirements. One of those requirements is using high-quality datasets to minimize risks and discriminatory outcomes.

Furthermore, the dilemmas in applying artificial intelligence methods in digital palaeography, as presented in [23], also reflect our difficulties in using artificial intelligence techniques for critical writer identification applications. In our view, a system that could be used in forensics and as evidence in court trials must be easily explainable, understood, and most importantly, trusted.

Directional methods [24]–[28] fulfil the above criteria since they can be easily explained, understood and ultimately trusted. Moreover, they are computationally efficient and fast and could be even run on mobile devices if such a need arises. Finally, their requirements for training data is minimal since only one page of handwritten text is sufficient, in most cases, to capture the necessary characteristics, or the feature vector, of a writer.

In our work on Skeleton Hinge Distribution [28], the skeleton information was used to make the feature extraction faster. However, by considering only the Skeleton, a big part of the available pixel information is discarded. This choice has motivated us to investigate if any additional information that could help identify the writer lies in discarded information.

Furthermore, our work on Detecting the Main Body size [29] made apparent that the Main Body size fluctuations could be observed even in a single text written by one writer. This observation motivated us to utilize this information and explore its contribution towards identifying the writer. Finally, on [20], they observed that neural networks trained on grey-scale images performed better than neural networks trained on binarized and contour images indicating that texture information

is an essential factor for writer identification. This observation motivated us to investigate if the same can be observed in Directional methods.

In a nutshell, the objectives of this thesis are as follows

Objective 1: We aim to make advancements in the preprocessing of handwritten document images that will allow us to reduce the noise and extract valuable characteristics of the text.

Objective 2: We aim to advance directional feature extraction techniques and propose some new feature extraction methods.

Objective 3: We aim to experiment with various matching techniques for our features to understand better how the different matching techniques affect identification accuracy.

Objective 4: We aim to evaluate the choices made in our work regarding the skeletonization process and find out if there is a loss of information and the effect it has on performance.

Objective 5: We aim to experiment with pixel intensity and character size fluctuations to understand better how they affect identification accuracy.

### **1.3 Main Assumptions**

The written text consists of several pen strokes applied with some force on a medium like paper. While those ink strokes represent a single line to a human observer, the same ink stroke is digitized into several pixel lines. To make things worse, differences in pen ball size and the angle or surface of writing may produce significant variations in the number of pixel lines produced during the digitization process and differences in the character sizes.

The primary assumption done in this work is that all stroke widths, i.e., line thickness, should be the same size. Practically this means that an attempt is made to condense all the writing information in 1-pixel width strokes.

Furthermore, an assumption is made that even if all the available information is used in 1-pixel width fragments, the accuracy should not significantly deviate from the Skeleton Hinge technique accuracy.

Similarly, an assumption is made that the main body size variance affects the identification accuracy since Hinge angles are related to the size of characters. Imagine, for example, the character "o" with two different main body sizes. The first can be represented by capital "O" and the second with a small "o". The directional angle of writing on the small "o" is smaller than the directional angle of writing on the capital "O".

Moreover, an assumption is made that noise produced by the writer could affect identification accuracy. This kind of noise either consists of the writers attempt to erase with ink what he has written by mistake or smaller ink stains that resemble salt and pepper noise.

Finally, an assumption is made that the pressure applied to the medium by the writer can also affect accuracy. Since this work deals with offline writer identification, a further assumption is that the pressure can be represented by pixel intensity on the grey-scale document image.

### **1.4 Contributions**

In this work, several directional features and combinations of directional features with model-based features are presented. Specifically, several improvements of a statistical directional feature, the edge hinge distribution, are attempted in novel contributions as the Skeleton Hinge Distribution, the Weighted Skeleton Hinge Distribution, the Quantized Skeleton Hinge Distribution, the Directional Stroke Run Length Distribution and the Edge Skeleton Hinge

combination. Furthermore, the combination of the Skeleton Hinge Distribution feature with a model-based feature is explored based on a codebook of graphemes.

Novel contributions related to the preprocessing of the document images and the extraction of valuable characteristics are presented. More specifically, two techniques are presented for Main Body Size estimation, a characteristic with application in a broad range of document image analysis fields. One measures the Main Body size directly, while the other first estimates the baselines. Both methods are segmentation free. Finally, to give more objective results, experimental results are presented over a small collection of 10 printed documents and a collection of handwritten text.

Furthermore, a technique for text localization is presented, which takes advantage of the fact that text should present some contrast in comparison with the background to be distinguished by the human eye. First, a procedure of binarization is applied to create appropriate images for text detection. Next, the connected components of the image are extracted, and some heuristic rules are applied to identify areas containing text. Finally, a postprocessing step is applied to clean the document image from the noise that is not part of the text.

## 1.5 Overview

In chapter 2, state of the art in writer identification is presented. Then, an overview of the anatomy of the handwritten document image is given. Finally, significant terms and techniques related to document image analysis, in general, will be presented.

In chapter 3, statistical and model-based features used for writer identification are presented. Individually, Edge Direction Distribution, Edge Hinge Distribution and Edge Hinge Combinations, along with our contributions, the Skeleton Hinge Distribution, the Weighted Skeleton Hinge Distribution, the Quantized Skeleton Hinge Distribution, the Directional Stroke Run Length Distribution and the Edge Skeleton Hinge combination are presented. Furthermore, a Model-Based feature that only considers closed areas of the characters is presented.

In chapter 4, two novel approaches for estimating the Main Body size and a technique for noise-cleaning through text localization will be presented.

In chapter 5, the data set used to evaluate this work is presented along with experimental results from our feature extraction techniques. More specifically, experimental results on Skeleton Hinge Distribution using the Nearest Neighbour classifier, K-means, Hierarchical Cluster Tree, K-Nearest Neighbours and Support Vector Machines are presented. Moreover, results on Quantized Skeleton Hinge Distribution, Weighted Skelton Hinge Distribution, Run Length Directional Hinge and Edge Skeleton Hinge Combinations, and Codebook of Graphemes combined with Skeleton Hinge Distribution are presented.

Finally, in Chapter 6, an interpretation of the feature vector characteristics produced by the directional methods mentioned above is attempted. Furthermore, an explanation of how matching is achieved and what happens on false identifications is provided. Furthermore, a discussion about writer identification techniques is provided, and finally, our conclusions are drawn.

## 2. State Of The Art

In this section, a review of recent papers published on the topics of writer identification and some from writer verification are presented. Writer verification was chosen because some of the feature extraction techniques developed for writer verification can also be used in writer identification. Several approaches exist in the literature for writer identification. First, works that entail a classical method, i.e. statistical or model-based strategies, are reviewed—followed by the most recent works based on artificial intelligence and deep learning.

Bulacu et al. [24] proposed the Edge Directional Distribution (EDD) and the Edge-Hinge Distribution (EHD) features. While Edge directional distribution considers the direction of a single edge fragment, the Edge-Hinge distribution considers the directions of two edge fragments emerging from a central pixel of a sliding window. Next, the probability distribution of the directions detected is generated for every writer in the train data set and then for every writer in the test data set. Finally, the generated distributions from the test data set are matched against the generated distributions of the train data set using the nearest neighbourhood algorithm. Experimental results reported an accuracy of 35% for the Edge directional distribution and 63% for the Edge-Hinge directional distribution on Firemaker DB [14].

Laurens van der Maaten et al. [25] suggested an improved Edge Hinge Directional feature, the Edge Hinge Combinations (EHC), by combining various sliding window sizes in a single feature. Experimental results achieved an identification accuracy of 81% on Firemaker DB.

Brink et al. [26] suggested the Quill feature, a probability distribution of the local relation between ink direction ( $\phi$ ) and ink width ( $w$ ). Furthermore, the Quill-hinge feature was suggested, which records the ink width in conjunction with the two directions ( $\phi_1$ ) and ( $\phi_2$ ). While the Quill feature achieved 71% accuracy, the Quill-hinge achieved 86% accuracy, both on Firemaker DB.

He and Schomaker [27] proposed two directional features. The CoHinge feature is defined as the joint distribution of the Hinge kernel on two different pixels of writing contours, and the QuadHinge feature, defined as the joint distribution of angles, along with the curvature information of contour fragments. The CoHinge feature was used in the ICDAR 2017 writer identification competition [15] in the method Groningen, achieving an accuracy of 76.1%.

Finally, He et al. [30] proposed a model-based approach for junction detection using the stroke length distribution in every direction around a reference point inside the ink of texts. A codebook-based representation of the junctions detected is constructed and used for writer identification achieving an accuracy of 80.6% on the Firemaker DB.

Said et al. [12] proposed a text-independent approach for writer identification that derives writer-specific texture features using multi-channel Gabor filtering and Gray-Scale Co-occurrence Matrices. This method requires uniform blocks of the text created by word deskewing, predefined thresholds of the distance between text lines, words and text padding. Two small sets of 20 writers, with a large number of 25 samples of handwriting text per writer, are used in the evaluation. The Nearest-centroid classification using weighted Euclidean distance and Gabor features achieved an accuracy of 96%. One of the main issues of this approach is the large number of sample pages required per writer.

Zois and Anastassopoulos [31] proposed a method for writer identification using a single word. They apply image thresholding and curve thinning, resample the horizontal projection profiles, and then use morphological operators to obtain 20-dimensional feature vectors classified using a Bayesian classifier. Experiments were performed on a single word, the word "characteristic",



written 45 times by each writer, both in English and Greek. The dataset consisted of 50 different writers. The reported accuracy of this method is 95%.

Srihari et al. [32], on a writer verification approach, proposed a considerable number of features divided into two categories. Macro-features, which operate at document, paragraph and word level. Also, Micro-features, which operate at word and character levels. The macro-features are based on grey-level entropy and threshold, number of ink pixels, number of interior and exterior contours, number of 4-direction slope components, average height and slant, paragraph aspect ratio and indentation, word length and upper and lower zone ratio. The Micro-features utilize gradient, structural, and concavity attributes. The proposed system considers two handwritten document images and outputs a decision made if the two input images are from the same writer or a different one. Experimental results were performed on a dataset containing 1000 writers who copied a fixed text of 156 words (the CEDAR letter). This writer verification method achieved on same writer accuracy of 94.6 % while different writer accuracy was 97.6 %.

Bensefia et al. [33] use graphemes generated by a handwriting segmentation method to encode the individual characteristics of handwriting. These graphemes are then clustered to define a feature space common for the document set. Finally, grapheme clustering is used to define a feature space common for all documents in the dataset. The reported experiment results achieved an accuracy of 90 % on a dataset consisting of 88 writers (PSI) and 68 % on a dataset of 150 writers (IAM).

Schomaker et al. [34] compute fragments of connected-component contour classified to identify the writer. Next, a codebook of graphemes is generated by training a Kohonem SOFM on many grapheme contours. Later, graphemes are extracted from each document and matched with the graphemes in the codebook. Finally, a histogram of graphemes for every document is generated. Experimental results achieved an accuracy of 95 % on ten writers and 83 % on 215 writers. When combined with Edge Directional features, 97% accuracy is achieved.

Laurens van der Maaten et al. [25] improved edge hinge directional features using a combination of window sizes while combining these features with a codebook of graphemes achieved 97% identification accuracy. In addition, the edge hinge combinations methodology proposed achieved 81% identification accuracy on the Firemaker dataset, which consists of 250 writers.

Schlapbach and Bunke [35] used HMM to identify and verify writers. Single writer recognizers are specialized by training using only handwriting originating from the chosen writer. More specifically, the output log-likelihood scores of the HMMs were used to identify the writer on handwritten text lines of varying content. This method achieved 96% identification accuracy and 2.5% error in verification accuracy as reported on a subset of the IAM database containing 100 writers, five handwritten pages per writer.

Pervouchine and Leedham [36] proposed a writer identification scheme based on high frequent characters. The high frequent characters ('f', 'd', 'y', 'th') are identified and used to determine the writer. Characteristics like height, width, height to width ratio, height of ascenders and descenders, stroke angle, slant angle and others. Experimental results achieved an identification accuracy of 58 %.

Bar-Yosef et al. [37] proposed a method for writer identification applied to historical Hebrew calligraphy documents based on topological features. While his approach seems similar to Pervouchine and Leedham approach, they use three high frequent Hebrew characters only to identify the writer. Connected components for tracing background, the convex hull of the characters, the ratio between background and convex hull, concavity, compactness are some of the features used in this approach. The reported experimental results achieved an accuracy of 100 % on 34 writers.

Li et al. [38] proposed a method for text-independent online handwriting writer identification. They used the feature vector of hierarchical structure in shape primitives and the dynamic and static feature for writer identification for English and Chinese documents. Experimental results achieved an identification rate of 91.5% with datasets in Chinese text and 93.6% in English text. It is an exciting methodology with the drawback that it cannot be applied to offline writer identification because the direction of the stroke of the writer is unknown.

He et al. [39] developed a technique for offline, text-independent writer identification of Chinese handwriting documents. He applied the Gabor filter to extract features from the text and incorporated a Hidden Markov Tree in the wavelet domain. Experimental results achieved an accuracy of 36.4% on a dataset of 500 writers with two handwritten text documents each.

Yan et al. [40] utilize spectral features using Fast Fourier Transformation to identify the writer of Chinese text. The identification rate achieved in this method is 64 % on 100 writers.

Bulacu et al. [41] developed a text-independent writer identification method for Arabic text. They use textural and allographic features to define a probability distribution function and apply the nearest neighbourhood classifier using them as a distance measure.

Al-Dmour et al. [42] identify writers in Arabic using different feature extraction methods such as hybrid spectral-statistical measures (SSMs), multiple-channel (Gabor) filters, and the grey-level co-occurrence matrix (GLCM) were verified to find the best subset of features. In addition, they experimented with various classifiers to rank the extracted features.

Wu et al. [43] proposed a method based on scale-invariant feature transform (SIFT) in three stages of training, enrollment, and identification. First, an isotropic LoG filter is utilized to segment the image to word regions from where SIFT descriptors are extracted into a codebook. Second, scale and orientations are used to construct an orientation histogram. Finally, a distance metric is used for matching. Experimental results on the Firemaker dataset achieved 92.4% accuracy.

Nicolaou et al. [44] developed a generic text-as-texture classification scheme where Sparse Radial Sampling Local Binary Patterns are constructed in histograms for different radius. In their Barcelona variation used in ICDAR 2017 writer identification competition [15], they used 12 radii to create histograms normalized with a PCA transform.

Mohammed et al. [45] proposed the Local Naïve Bayes Nearest-Neighbour (Local NBNN) classifier. In this method, the SIFT algorithm is used to detect and describe critical points with a constrain that considers the particularity of handwriting patterns and prevents irrelevant points to be matched. Normalization is also proposed to cope with unbalanced data. In their Hamburg variation used in the ICDAR 2017 writer identification competition [14], they used NBNN instead of the local NBNN without normalization.

Newell et al. [46] proposed the oriented Basic Image Feature Columns (oBIF Columns) that entail a mixture of allograph and texture-based methods that encode a writer's deviation from the mean encoding population of writers with the Delta Encoding.

Abdeljalil et al. [47] developed a method that uses oriented Basic Image Features (oBIFs) that labels locations in the document images into seven symmetry classes for several orientations. Column histograms are constructed, and a distance metric is used for matching. For example, in their Tebessa I and II variations used in ICDAR 2017 writer identification competition [15], they used city block distance.

Nadia et al. [48] applied 16 Gabor filters for handwriting texture analysis, while Gazzah et al. [49] applied spatial-temporal textural analysis. Al-Ma'adeed et al. [50] identify Arabic writers using only 16 words. They utilize edge-based directional features and three edge-direction distributions of different sizes.

Chahi et al. [51] suggested using a Block Wise Local Binary Count (BW-LBC) operator, which represented the writer by a set of histograms calculated from all the connected components in the text and is based on the occurrence distribution of pixels in small blocks. In addition, the nearest-neighbour classification using the Hamming distance was utilized for matching.

Chahi et al. [52] proposed Cross multi-scale Locally encoded Gradient Patterns (CLGP). This new feature extraction technique that represents better salient local writing structure operates at connected component sub-images of the writing sample. Then CLGP histogram feature vectors are computed from all these observation regions in all writing samples, and the Nearest Neighbor Classifier is used for matching. Accuracy results reported in this work for the Firemaker database achieved an accuracy of 97.60%, showing that traditional methods are still helpful for writer identification.

Fiel and Sablating [16] suggested a convolutional neural network (CNN) method for writer identification. A CNN-based feature vector was generated for each writer compared with the precalculated feature vectors stored in the database using nearest neighbour classification.

Xing and Qiao [53] proposed DeepWriter, a deep multi-stream CNN that takes local handwritten patches as input and is trained with softmax classification loss.

Tang and Wu [21] suggested using a CNN and joint Bayesian at two stages, feature extraction and writer identification. In the first stage, and because much data is needed to train an effective CNN, an augmentation technique generates thousands of handwriting images for each writer. These generated images are then used to train the CNN model while the joint Bayesian method is utilized for writer identification.

Khan et al. [54] suggested an offline text-independent writer identification system, which combined SIFT (Scale Invariant Feature Transform) and RootSIFT descriptors in a set of Gaussian mixture models (GMM). They reported accuracy of 97.98% on the Firemaker dataset.

He and Schomaker [18] suggested using an end-to-end multi-task neural network with several adaptive convolutional layers with two types of information. Explicit information includes data like lexical content or word length and implicit attributes such as the author's identity. Their method performs writer identification on word level by resizing all word images to  $120 \times 40 \times 1$ .

He and Schomaker [19], in a later work, proposed FragNet. This deep neural network entails two pathways: a feature pyramid that is first used to extract feature maps and then a fragment pathway based on fragments extracted from the input image and the feature maps from the feature pyramid. In this work, word images were used to achieve writer identification on the word level. Their method achieved 57.5% accuracy on word images from the Firemaker dataset.

Finally, He and Schomaker [20] suggested the global-context residual recurrent neural network (GR-RNN) method. This work utilizes an end-to-end neural network that jointly integrates global-context information and a sequence of local fragment-based features. A global average pooling step is used at the tail of the neural network to acquire the global-context information, while a low-level deep feature map is used to extract the local fragment-based features. A recurrent neural network (RNN) is used to model the spatial relationship between the sequence of fragments and to strengthen the discriminative ability of the local fragment features. They reported an accuracy of 98.8 % on the Firemaker Dataset that is the best performance reported on the literature for the Firemaker Dataset.

### 3. Handwritten Document Image

#### 3.1 Handwritten Document Image Anatomy

Many characteristics can describe handwritten documents. First, the characters and words have unusual shapes and sizes. Furthermore, their layouts and the skew of the text are not uniform and depend on the writer. Moreover, the text lines do not follow a straight line but tend to have a curvature. Also, text lines may interfere with each other or might be physically connected with other lines. Finally, the interline spacing is not uniform. For an example of handwritten documents with the above problems, see Fig. 1 and 2.

While all the above are considered a problem for tasks like the automatic reading of these documents, they are regarded as features for writer identification since they can reveal the specific writer of the document.

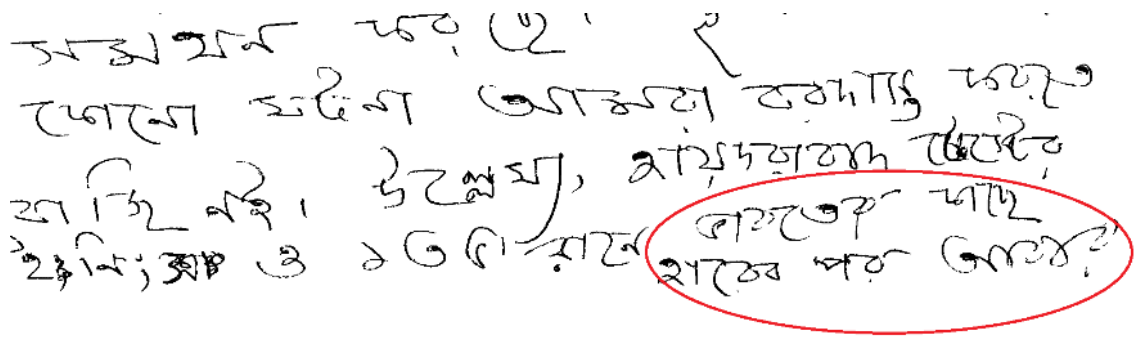


Figure 1. Example of a part of a handwritten historical document image from the ICDAR 2013 Handwriting Segmentation Contest [55] benchmark dataset with interfering lines (ellipse), non-uniform skew, non-uniform interlines spacing and text lines with curvature.

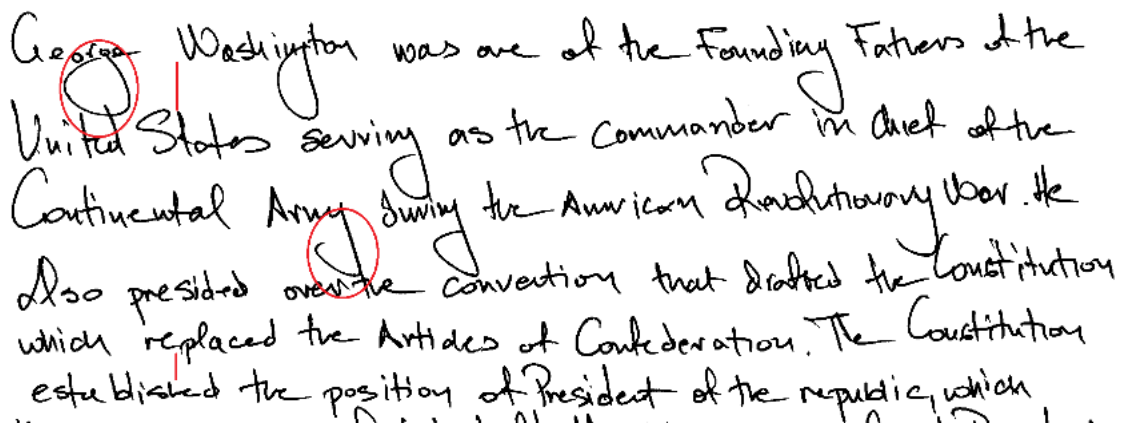


Figure 2. Example of a part of a handwritten historical document image from the ICDAR 2013 Handwriting Segmentation Contest benchmark dataset with connected lines (circles), non-uniform skew and non-uniform interline spacing (line).

Handwritten documents do not have a standard form of writing or any uniform layout. The text line structure is the most dominant structure of these documents. A handwritten document image

can be viewed as a text area that consists of text lines. Every text line also consists of one or more words, while every word can be seen as a set of characters in order. Characters, in their turn, consist of black pixels. This work assumes that document images have a white background black foreground (text).

While humans can easily distinguish the text lines, the mechanism of this inherent ability is a fantastic feature of the human brain that is still an unsolved problem for computer algorithms. Even when the handwritten document image is seen at a significant distance, while the characters and the words are still blurry, the human brain can still distinguish the distinct lines that form the text. For example, see Fig. 3 and Fig. 4, two images from the ICDAR 2013 Handwriting Segmentation Contest [55] are scaled to 5% of the original image size. Thus, while it is still hard for a human to read the exact text, it is easy to segment the different text lines.

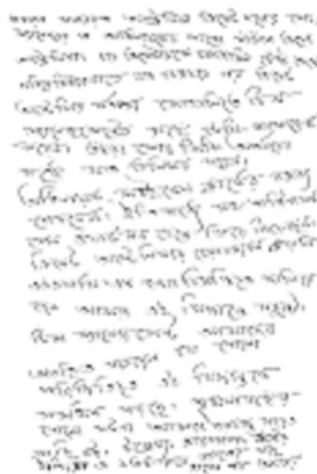


Figure 3. Example of handwritten historical document images from the ICDAR 2013 Handwriting Segmentation Contest benchmark dataset, scaled to 5% of the original size. Text lines can be distinguished from a human, even on this scale.



Figure 4. Example of handwritten historical document images from the ICDAR 2013 Handwriting Segmentation Contest [10] benchmark dataset, scaled to 5% of the original size. Text lines can be distinguished from a human, even on this scale.

### 3.2 Terms Definition

In this section, the different terms associated with the physical structure of handwritten documents are presented. For graphical representations, please see Fig. 5 and Fig. 6

- A stroke is considered the movement of a writing instrument (pen) on a writing surface (paper)
- The baseline of text is the imaginary line that follows the lower part of the characters.
- The median line of text is the imaginary line that follows the upper part of the character.
- The upper line of text is the imaginary line that follows the upper parts of ascenders.
- The lower line of text is the imaginary line that follows the lower parts of descenders.
- The main body of the text is the size between the baseline and the median line.
- The ascenders are the parts of lowercase characters that lie above the median line.
- The descenders are the parts of lowercase characters that lie below the baseline.
- A component is considered a single character or several connected characters that form a word in this work. Component, in a more general term, is regarded as the connected pixels with similar intensity values.
- Overlapping components are the ascenders or descenders that are in the region of the line above or below.
- Touching components means the ascenders or descenders are physically connected with a part of the text line above or below.

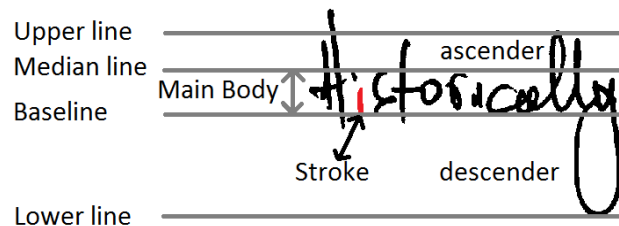


Figure 5. Upper line, Median line, Baseline, Lower line, a single stroke, ascenders and descenders.

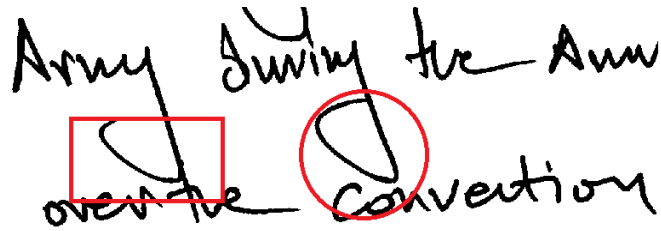


Figure 6. Square: touching components. Circle: overlapping components

### 3.3 Document Image Analysis

In this section, an attempt is made to give all the necessary definitions for the methods described in the next chapter, to be more easily understandable. A basic introduction of what a digital image is, is given. Furthermore, some exciting image analysis techniques like image binarization, edge detection, Gabor filters, skeletonization, connected components, contour tracing, Main Body, run lengths, Fourier transformation, and text localization will be briefly presented.

#### 3.3.1 Digital Image

When a document image is scanned, it is transformed, through a process of digitization, into a digital image. This digital image is, in fact, a numeric representation of a two-dimensional matrix if the image is digitized to contain only the grayscale representation. Alternatively, it can be represented to a three-dimensional matrix if the image is digitized to include all the available colour information. For the digitization process, the image is first sampled on a discrete grid, and then each sample, or pixel, is quantized using a finite number of bits. Finally, a computer processes the digitized image. For example, in Fig.7, a document image fragment is presented with the word "The".

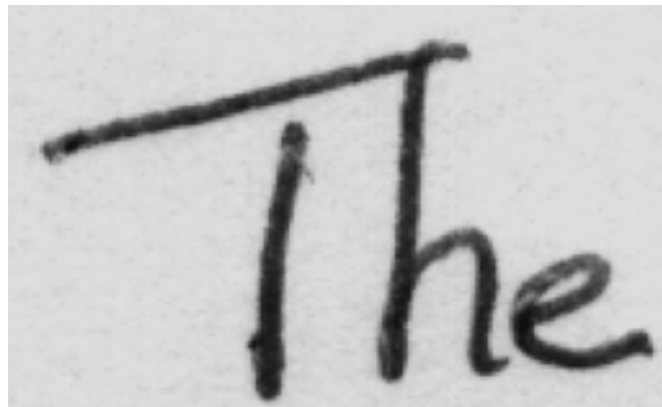


Figure 7. Fragment of a digital image with the word "The"

In scanning or digitization in general, the image is viewed as small elements, called pixels. A matrix of pixel intensity is stored that can later represent the scanned image. For example, if a zoom-in on a digital image is attempted, at some point, the distinction between the different pixels the image consists, can be observed. For example, see Fig 8.

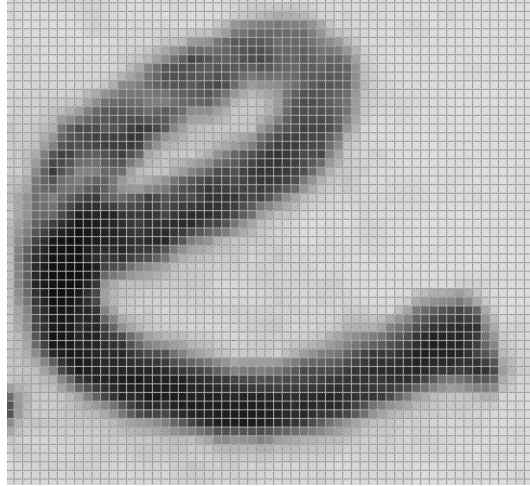


Figure 8. Fragment of a digital image with the character “e”, zoomed to the pixel level

This pixel intensity matrix is, in fact, a numerical matrix. Each pixel intensity value stored in this matrix represents how bright a pixel will appear on a screen. The higher the intensity value of a pixel is, the whiter it will look. Grayscale images use 8-bit integers to store pixel values, meaning that a pixel can be represented by a numerical value between 0 and 255. In Fig. 9, the character "e" is represented in a pixel intensity matrix. The same character "e" as viewed in Fig. 7 and Fig 8 only scaled at 30 %.

220	221	221	222	222	221	221	218	219	220	221	221
218	219	219	221	221	221	221	220	218	220	220	222
216	221	222	221	223	220	219	219	221	222	220	222
216	215	220	222	221	224	224	221	220	221	222	219
219	222	223	177	141	132	170	218	218	217	218	219
201	140	96	83	68	97	98	137	220	220	219	220
118	74	75	92	136	115	83	95	211	219	219	220
102	102	128	189	210	105	71	111	217	214	219	222
67	171	212	189	125	60	60	159	224	221	221	220
194	192	130	78	48	46	110	203	215	219	220	219
105	79	48	50	67	127	204	211	214	213	216	218
46	37	55	102	186	218	221	218	212	219	221	222
61	126	190	210	209	210	216	215	216	220	220	222
191	207	207	216	209	209	210	213	223	225	220	212
218	216	213	212	208	208	216	208	218	182	99	71
145	181	208	220	211	214	195	152	115	72	28	24
34	51	87	133	140	117	81	65	38	30	37	52
22	18	21	26	30	38	32	33	63	110	176	191
149	116	69	44	44	66	96	140	195	211	213	215
208	208	211	198	195	207	210	216	211	214	212	216
214	211	207	214	214	216	213	218	216	215	222	217
216	216	219	215	214	214	218	220	219	219	221	219
211	215	218	218	209	220	215	216	215	218	212	215
217	218	219	216	216	219	216	215	214	219	217	214

Figure 9. the character “e” represented in a pixel intensity matrix

### 3.3.2 Binarization

An image can be binarized using a threshold [56] to consist only of values 1 or 0, white or black. In Fig. 10, a binarization example that uses a threshold of 150 is presented. In this example, values smaller than 150 are set to 0, while values greater or equal to 150 are set to 1. This grayscale image will be transformed into a binary one with the above process, although this is just one



method for binarizing an image using a global threshold. More complicated methods exist that use adaptive [57] thresholding and other techniques. In Fig. 10, an example of the image in Fig. 9, binarized using a global threshold, is presented.

1	1	1	1	1	1	1	1	1	1	1
1	1	1	1	1	1	1	1	1	1	1
1	1	1	1	0	0	0	0	0	1	1
1	1	0	0	0	0	1	0	0	0	1
1	0	0	0	1	1	1	0	0	0	1
0	0	0	1	1	1	0	0	0	1	1
0	0	1	1	1	0	0	0	0	1	1
0	0	0	0	0	0	0	0	1	1	1
0	0	0	0	0	0	1	1	1	1	1
0	0	0	0	1	1	1	1	1	1	1
0	1	1	1	1	1	1	1	1	1	1
0	1	1	1	1	1	1	1	1	1	1
0	0	1	1	1	1	1	1	1	1	0
0	0	0	0	0	1	1	0	0	0	0
0	0	0	0	0	0	0	0	0	0	0
1	1	1	0	0	0	0	0	0	1	1
1	1	1	1	1	1	1	1	1	1	1
1	1	1	1	1	1	1	1	1	1	1
1	1	1	1	1	1	1	1	1	1	1
1	1	1	1	1	1	1	1	1	1	1
1	1	1	1	1	1	1	1	1	1	1
1	1	1	1	1	1	1	1	1	1	1

Figure 10. The character "e" is represented in a binary pixel intensity matrix

Binarization is a ubiquitous pre-processing task of image processing, which reduces the size of the image and allows fast and easy calculations and further processing of an image. It is considered a mandatory task in many computer vision systems [58], and several works have used binarization as an aid for text detection [59]–[62].

### 3.3.3 Edge Detection

Edge detection [63] is the process of identifying the specific points in a digital image where the image brightness suddenly changes or has discontinuities. Those points are typically organized into a set of curved line segments named edges. With edge detection, the boundaries of objects in an image are indicated, making the methods of edge detection a fundamental tool in image processing, machine vision and computer vision. The output of an edge detection algorithm is a binary image, with only the edge pixels having a value of 1. For an example of applying an edge detection algorithm, and more specifically Sobel edge detection, see Fig 11.



Figure 11. The output of edge detection on the image of Fig. 7.

### 3.3.4 Gabor Filter

Gabor filters [64] are orientation-sensitive filters used for texture analysis. They typically traverse an image in multiple directions. A Gabor filter, set in a direction, will give a strong output for locations of the target images that have structures in this given direction. For example, suppose the target image is made of a periodic grating in a diagonal direction. In that case, a Gabor filter set at a direction will give a strong output only if its direction matches one of the gratings. Gabor filters have also been used to localize and extract edges since edges are composed of higher frequency components, whereas other image regions are relatively smooth. Frequency and orientation representations of Gabor filters are similar to those of the human visual perception, and they are appropriate for texture identification and representation. Gabor filters have many practical applications. They are primarily used in character recognition and fingerprint enhancement and also writer identification systems. For example, see Fig. 12.

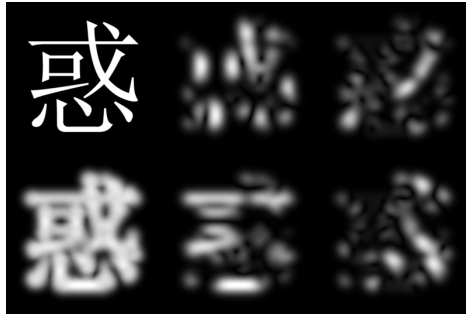


Figure 12. Top left: Original Chinese character. Top middle: Orientation = 0 degree. Top right: Orientation = 45 degree. Bottom middle: Orientation = 90 degree. Bottom right: Orientation = 135 degree. Bottom left: Superposition of all four orientations.

### 3.3.5 Skeletonization

A topological skeleton [65] is a thin version of the shapes found in a digital image. The skeleton usually highlights the geometrical and topological properties of a shape. These properties include its length, direction, width, topology and connectivity. Thus, the skeleton can efficiently represent that shape since it contains all the necessary information to reconstruct it. In this work, skeletonization is referred to as thinning the characters, so only their skeletons are left. Skeletons have been utilized in various fields, like image analysis, computer vision, and digital image processing, including applications for fingerprint recognition, optical character recognition, binary image compression, and pattern recognition. An example of the skeleton of the word “The” is given in Fig. 13.

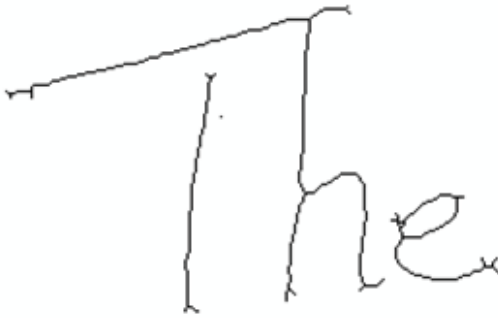


Figure 13. The output of skeletonization on the image of Fig. 7.

### 3.3.6 Connected Components

Connected components are groups of pixels that share similar pixel intensity values and are connected [66]. Connected component algorithms work by traversing an image pixel-by-pixel (from top to bottom and left to right) to identify connected pixel regions, i.e. regions of adjacent pixels that share the same set of intensity values. For example, an algorithm can be set to check for a 4-connectivity connected component or an 8-connectivity connected component Fig. 14. 4-connectivity algorithms check the upper, the bottom, the left, and the right neighbour pixel for the same intensity. 8-connectivity checks the entire neighbourhood of the central pixel for pixels with the same intensity.

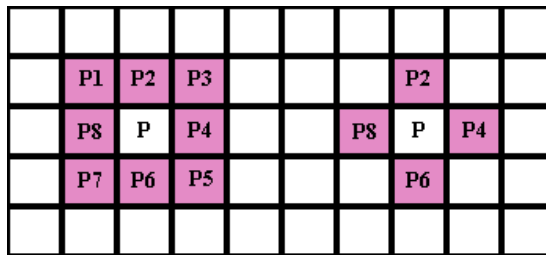


Figure 14. left: 8-connectivity. Also called a Moore neighbourhood. right: 4-connectivity

Only connected pixels with a numeric value "1" will be considered in the same group for a binary image. While on grayscale images, a range of intensity values is considered. Each group of connected components is labelled, either with an id or with a different colour.

The connected components technique is advantageous in document image analysis because each character can be categorized as a connected component with a given label.

### 3.3.7 Contour Tracing

Contour tracing [67] output might look almost the same as edge detection algorithms; however, edge detection algorithms try to find points that are at the extreme of the image gradient in the direction of the gradient, with the edge pixels, pointing out a significant difference between neighbouring pixels. Contour tracing tries to find the contour, i.e. the boundaries, of an object. Contours need to be closed curves to map precisely the boundaries of any given object, while edge detection does not require closed curve edges. Usually, objects are first identified through a connected component tracing, and then the contour of every object is extracted. A complete

contour includes both the exterior contour and the interior contour. Interior contours are harder to detect because they reside in character closed areas. For example, a complete contour of character A is given in Fig 15.

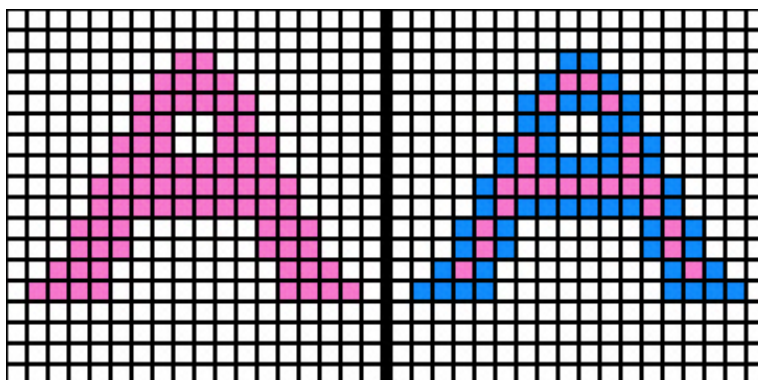


Figure 15. left: The character “A”. right: The complete contour of character “A”.

### 3.3.8 Main Body

Main Body [29] or core region size is a characteristic that is used quite often in most document image processing systems. As Main Body, it is considered the central part of the text, excluding ascenders and descenders (Fig.16). Most of the time, it is referred to words.



Figure 16. Word Main Body and baselines.

Main Body is a characteristic used in many systems that use image processing for various tasks in document images. It has been used in systems for OCR [68], [69], segmentation [70], [71], slant removal [72], dewarping [73], [74], word matching [75], indexing [76], word spotting [77]–[79], etc. All the above systems utilize the main body information and use it as a threshold or character size information, as it is directly related to the size of the characters, the document image resolution and the text orientation.

The Main Body size can also be utilized to get a rough estimation of the character width. Especially in [79], they mention: By mean width of the character, we consider the width of characters such as a, b, c, d, e, f and others, excluding the characters i,l,j,m,w that are either too narrow (i,l), or too broad (m,w). Although the character width differs between characters and writers, a rough estimation of the mean width could be made by accepting that characters present width equal to their height, excluding the ascenders and descenders height of the characters.

Considering all the above, we see that Main Body is crucial in document image processing systems. Thus, many techniques have been developed for calculating the Main Body.

### 3.3.9 Run Length Encoding

Run Length Encoding counts runs of data with the same value that occur in consecutive pixels. It is used primarily on binary images for various tasks, from data compression to skew detection and line segmentation. In binary images, two distinct types of run lengths exist. Black run Lengths, where consecutive pixels that are off (0) are counted and White Run Lengths where consecutive pixels that are on are counted. For example, the pixel sequence in Fig. 17 has a black run-length encoding of 2, 3, 7, 2, 3

001000100000001001000

Figure 17. An example of a pixel sequence with a black run length with values 2, 3, 7, 2, 3

### 3.3.10 Fourier Transformation

Fourier Transformation is a valuable image processing tool used to decompose an image into its sine and cosine components [80]. The output of a Fourier transformation is a complex number valued output image that represents the input image in the frequency domain. The input image is considered the spatial domain equivalent, and by spatial, it is meant the normal image space. In the Frequency domain image, each point represents a particular frequency contained in the spatial domain image.

The complex number valued output image produced by the Fourier Transform can be displayed with two images, the magnitude image and the phase image. The magnitude image contains most of the information of the geometric structure of the input image, and thus, in image processing, only the Magnitude of the Fourier Transform is displayed. However, for re-transforming the Fourier image into the correct spatial domain image after some processing in the frequency domain, both the Magnitude and phase of the Fourier image are required.

Furthermore, unlike a typical grayscale image in the spatial domain represented with pixel intensities between a range of 0 and 255, the Fourier domain image consists of a much higher range. Thus, to be sufficiently accurate, its values are usually calculated and stored in float values. The Fourier Transform can be found in various applications, such as image filtering, image analysis, image reconstruction and image compression. An example of the magnitudes of specific handwriting letters can be seen in Fig 18.

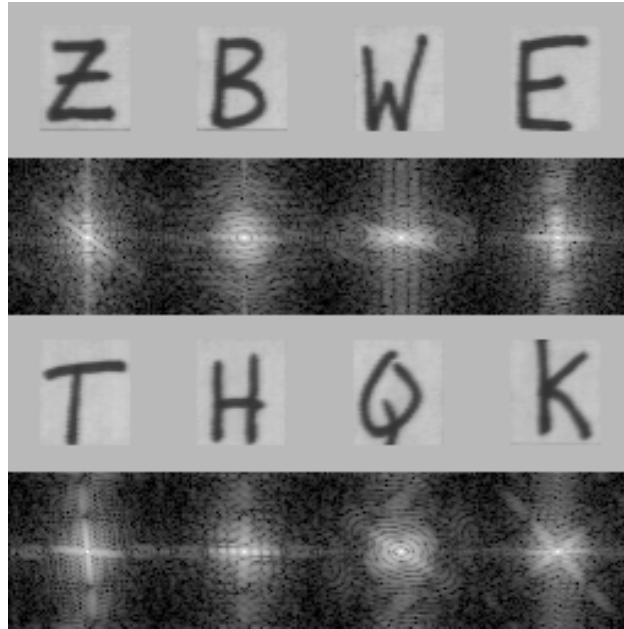


Figure 18. Handwritten characters, along with their Magnitude in the Fourier domain

### 3.3.11 Text Localization

Text localization is an old computer vision problem, which started to be studied in the '90s [81], and it involves the task of localizing text in images. Nowadays, efficient solutions to this problem are more useful than ever in robotics, smart cars, smartphones and other fields. Thus, many techniques have been proposed using connected components [82], edge detection [83], sliding windows [84], hybrid techniques [85], as well as other techniques [86]. Moreover, in the last years, four competitions have been organized on robust reading [87]–[90], which has motivated active research in this area.

## 4. Writer Identification Techniques

State of the art writer identification systems uses various techniques that use different feature types and classifier approaches to identify the writer. Features can have many types, statistical features where distribution is calculated, structural features where specific rules related to the text structure are applied, model-based features where the characters are treated like allographs or graphemes where the text is treated as texture and many others. Furthermore, features can be extracted from different levels of the text, like the macro-level that includes features from the entire document, paragraphs, lines or words and the micro-level that includes features from characters, parts of characters (graphemes) or pixels. On the other hand, classification approaches can be categorized into five types [91]: minimum distance classifiers, statistical classifiers, neural networks, fuzzy classifiers and syntactic classifiers.

In the scope of this work, a focus is given on statistical-textural directional features on the micro-level that are extracted using a Probability Distribution Function (PDF) and minimum distance classifiers. Furthermore, further experiments were performed using a combination of statistical-textural features with model-based features. Finally, statistical classifiers and neural networks were also considered.

The focus will be given to edge direction features [24], their advancements, edge hinge distribution, and edge hinge combinations [25]. Edge hinge distribution is reported to outperform all other statistical features while edge hinge combinations improve the previous method. An attempt is made [28] to improve the edge hinge combinations methodology using image skeleton, thus referring to this methodology as skeleton hinge distribution. Further improvements are also attempted on the skeleton hinge distribution on a weighted variation using the Main Body size at the pixel level. Furthermore, an attempt was made to utilize the pixel intensity information on a quantized version of the skeleton hinge approach. Furthermore, a novel approach on directional features is presented using Directional Stroke Run Length Hinge Distribution. Finally, a combination of the Edge Hinge Combinations Distribution with the Skeleton Hinge Distribution is presented.

While directional features distributions have good results, they are directly related to the writer's slant. The slant is a characteristic that can be easily forged. A combination of skeleton hinge distribution with a model-based one is presented to secure this method and improve the results. The model-based technique used in this thesis involves using predefined models of small strokes of handwriting called graphemes.

### 4.1 Statistical-Directional Features

#### 4.1.1 Edge-Direction Distribution

Edge-direction distribution, suggested by Bulacu et al. in [24], is the first and the most straightforward method in a family of techniques that consider statistical-directional features for the task of writer identification. In this method, extraction starts with edge detection. Edge detection generates a binary image in which only the edge pixels are kept. Next, each edge pixel is considered in the centre of a square neighbourhood. Then, all the pixels are checked, using logical AND operators, to all directions, emerged from the central pixel and end on the periphery of the neighbourhood, looking for the presence of another edge fragment (i.e. connected sequences of pixels). In Fig. 19, an edge image of the word "the" is presented. Furthermore, an example of a

square neighbourhood with a 4-pixel length edge fragment emerging from the central pixel with the direction of the fragment quantized in 12 directions is presented.

First, a histogram is created, using the count of all the verified direction instances, and then it is normalized to a probability distribution  $p(\varphi)$ . This distribution gives the possibility of finding an edge-based fragment oriented at the angle  $\varphi$  to the horizontal. Moreover, the most dominant direction in  $p(\varphi)$  corresponds to the slant of the handwritten text.

Some essential practical details that relate to the implementation of edge-direction distribution [24] should be mentioned. In order to avoid repetition, the algorithm only checks the upper two quadrants in the neighbourhood since it is hard to determine which way the writer "travelled" along with the found oriented edge fragment. In the experiments conducted in [24], they only considered 3,4 and 5 pixel-long fragments quantized in  $n=8,12$  and 16 directions, respectively. It is also worth mentioning that the edge detection method used does not generate 1-pixel wide edges, but instead edges that have a wide of 1 to 3 pixels. This practical detail introduced smoothing into the histogram computation, which they found advantageous in the experiments. For more details about algorithm options and results, see [24].

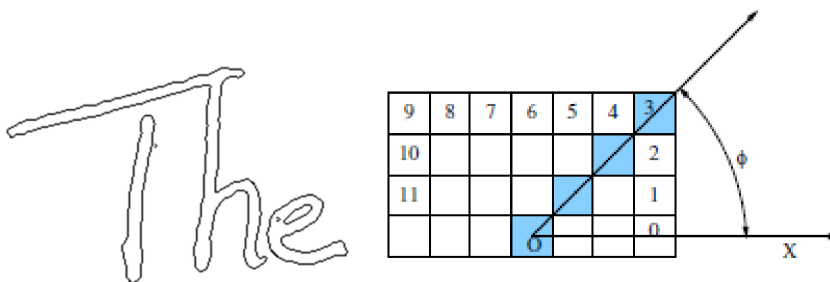


Figure 19. Extraction of edge-direction distribution.

#### 4.1.2 Edge-Hinge Distribution

Edge hinge distribution, also suggested by Bulacu et al. in [24], is an improved version of Edge-Direction distribution that considers not one but two edge fragments in the neighbourhood, emerging from the central pixel, and subsequently, compute the joint probability distribution of the orientations of the two fragments. This feature concerns the direction changes of a writing stroke in handwritten text. The edge-hinge distribution is extracted using a window that scans a binary handwriting image that contains only the edge information. When the central pixel of the window is "on", the two edge fragments emerging from this central pixel are considered only when  $\varphi_1 < \varphi_2$ . In Fig 20, an example of a window with a 4-pixel length edge fragment emerging from the central pixel with the direction of the fragment quantized in 24 directions is presented. The directions are measured and stored in pairs. A joint probability distribution  $p(\phi_1, \phi_2)$  is obtained over a large sample of pairs.

Furthermore, some practical details related to implementing the algorithm used [24] for this feature are worth mentioning. In this implementation, the edge detection algorithm does not produce 1-pixel wide edges, but instead, it produces 1-3-pixel wide edges. While in the edge-direction distribution, where only one edge fragment is checked, the edge detection did not consist of a limitation. In our case, two edge fragments must be checked. This consists of a limitation; thus, an extra constraint is implemented. The ends of the edge fragments are required to be separated by at



least one “non-edge” pixel. In the experiments conducted for this feature in [24], like the edge-direction distribution, only 3,4 and 5 pixel-long fragments are considered quantized in  $2n = 16, 24$  and 32 directions, respectively.

Furthermore, two more constraints are implemented in the algorithm that is worth mentioning. The first is that the  $\phi_1$  angle must be lower than the  $\phi_2$  angle. The second one is in cases where the ending pixels have a common side eliminated. For more details about algorithm options and results, see [24].

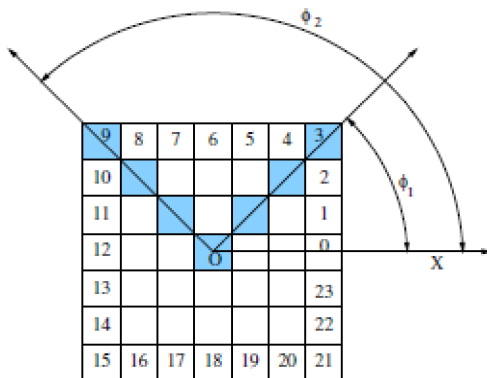


Figure 20. Edge Hinge Distribution Extraction

### 4.1.3 Edge-Hinge Combinations

The edge-hinge combinations, proposed by Van der Maaten et al. [25], improved the edge hinge distribution by considering multiple pixel length edge fragments (i.e. window sizes) instead of just one. Experimenting with combinations of edge hinge distributions and using various fragment lengths, they improved the results of writer identification by up to 12% compared with the edge-hinge distribution.

### 4.1.4 Skeleton-Hinge Distribution

The main problem with the current implementations is that the edges are usually close to each other, filling the feature matrix with duplicate and unnecessary data. Therefore, a simplified version of Edge-Hinge Combinations was used to consider the skeleton information of the image instead of the edge information to overcome that problem. Henceforth, this technique will be referred to as skeleton hinge distribution.

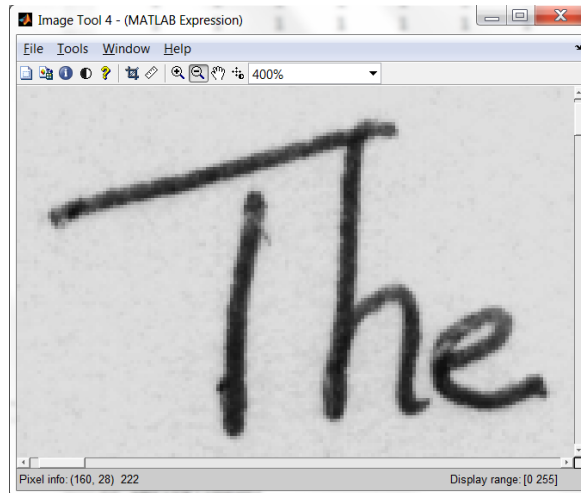


Figure 21. Handwritten digitized text

Usually, when something is written on paper (Fig.21), its thickness is considered a single line. However, when the image is digitized, the same trace of ink is translated into several pixel lines. By considering the edge hinge distribution, on an edge image (Fig. 22), much unnecessary information, like the bottom, or the side curves of the letters, is included in the feature vector. Furthermore, differences in line thickness from a variety of different pens may produce significant variations in the extracted features in both edge hinge distribution and edge hinge combinations. Therefore, the main suggestion in this work is that all stroke widths, i.e. line thickness, should be the same size. Thus, by skeletonizing the image, characters with a single-pixel width stroke are acquired.

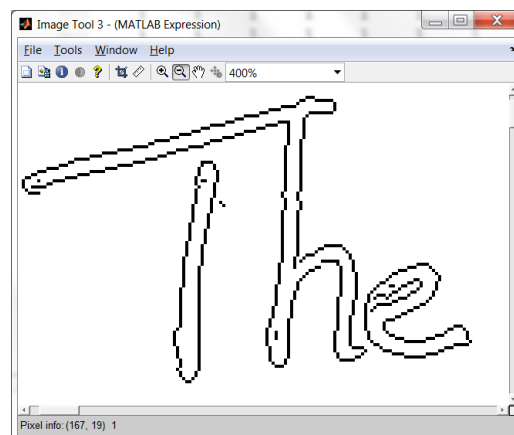


Figure 22. Edge image of handwritten text

On the skeleton hinge distribution, only the skeleton of the letters is considered (Fig.23), a simple structure that considers the basic required information to match the features to already known ones.

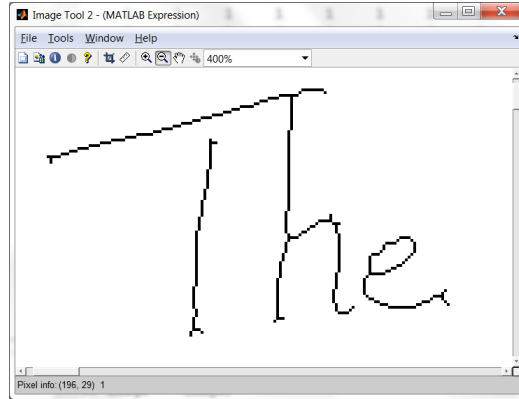


Figure 23. Skeleton image of handwritten text

The Skeleton Hinge distribution [28] belongs to a family of similar techniques like the edge hinge distribution and edge hinge combinations. The main idea is to locate two hinge line fragments emerging from a central pixel on a sliding window (Fig. 24) and store their directions in pairs. While on edge hinge distribution and edge hinge combinations, the edge information is used to locate hinge fragments, on skeleton hinge distribution, the skeleton information is used.

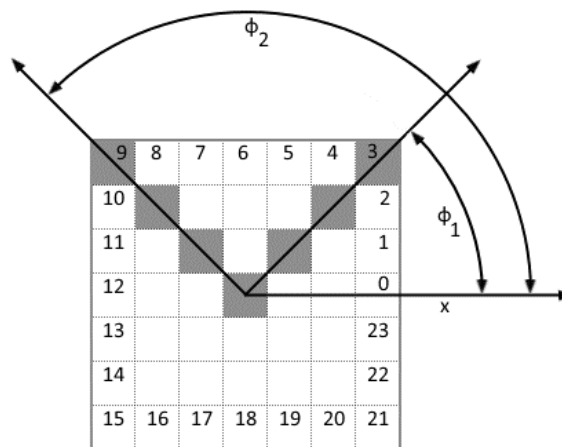


Figure 24. 4 pixels long Hinge line fragments, emerging from a central pixel, on a 7x7 window.

Skeleton Hinge distribution starts with the image skeleton extraction using a generic skeletonization approach [92]. Then a sliding window technique that uses several window sizes, each quantized in a different number of directions, checks for skeleton line fragments, which emerge from the central window pixel. Finally, their directions are measured and stored in pairs. Only skeleton line fragments with  $\phi_1 < \phi_2$  are counted and stored in pairs in a histogram. A joint probability distribution  $p(\phi_1, \phi_2)$  is obtained over a large sample of pairs. Finally, the probability distributions acquired by the various sliding window sizes are combined and considered for matching. For an instance of the Skeleton, Hinge Distribution extraction, see Fig. 25.

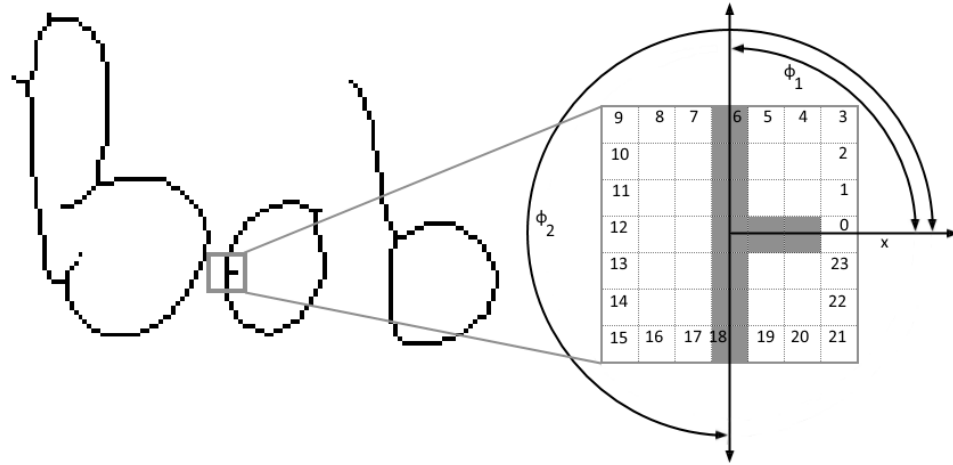


Figure 25. An instance of Skeleton Hinge distribution extraction with four pixels-long edge fragments on the part of the word "Bob".

The main ideas of edge hinge distribution and edge hinge combinations are present in the proposed technique. On the other hand, a significant improvement in the writer identification task results is observed by applying this methodology to a skeleton image.

It is essential to mention that the resulting feature matrix includes more compact information than the Edge Hinge Distribution feature matrix, and it is easier to compare two resulting matrices of test and train samples. Please check a successful application of the proposed system in figures 26,27,28, where some text samples are provided over their results. On the upper part of the figure, fragmented samples of the text are provided. The left text fragment is used as a training sample, and the right text fragment is used as a test sample. Both samples in each picture are from the same writer. Next, the surface of the Skeleton Hinge Distribution is presented. The left one corresponds to the training sample, while the right one to the test sample. Finally, on the lower part of the figure, the edge hinge combinations surface is presented. Again, the left one corresponds to the training sample and the right to the test sample.

Bob, David en  
van de landen  
USA, Holland,

Jan, een ve  
Hege- woest  
uit de lucht (

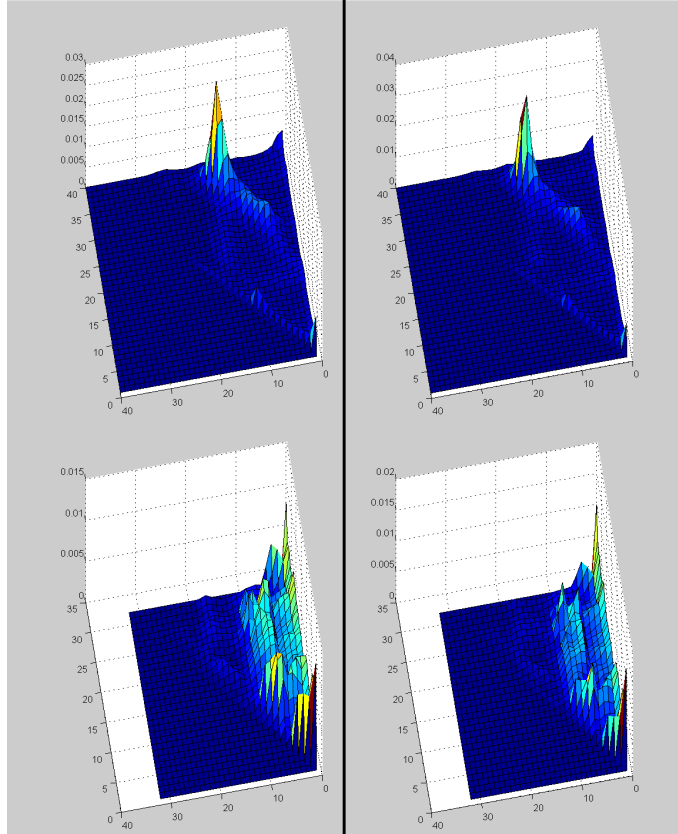


Figure 26. Text samples from the same writer along with skeleton hinge distribution feature surface (middle) and edge hinge combinations feature surface (bottom)

Bob, David er  
landen Egypte,  
Griekenland en

Een UFO landt  
honderd zijn zijn  
draakbrig figuur

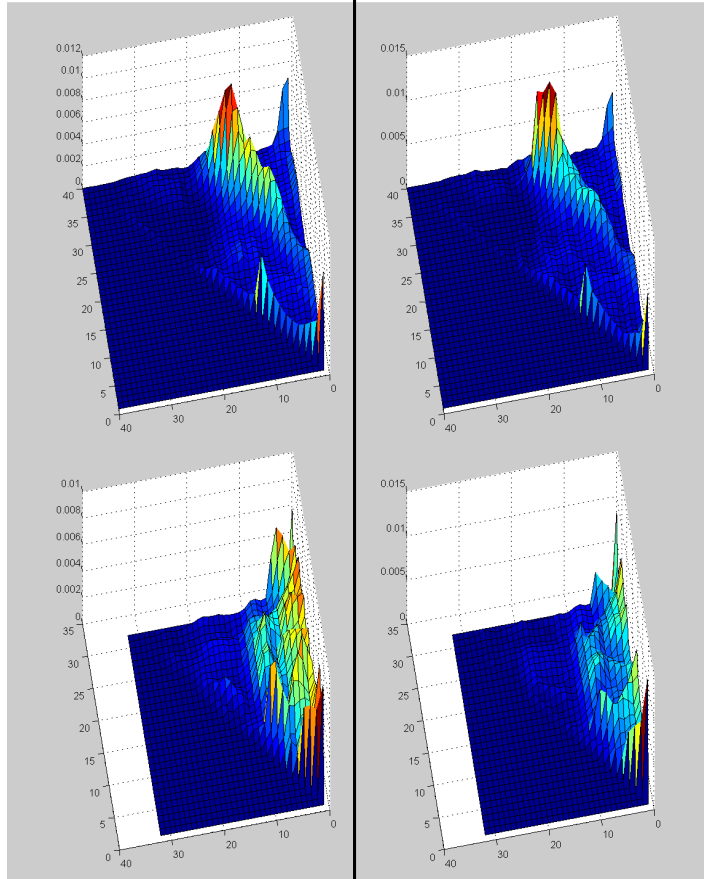


Figure 27. Text samples from the same writer along with skeleton hinge distribution feature surface (middle) and edge hinge combinations feature surface (bottom)

Bob, David en  
Egypte, Tapa  
en Canada.

Een vcatje,  
een vliegende  
Schotel stapt  
vcatje op z'a

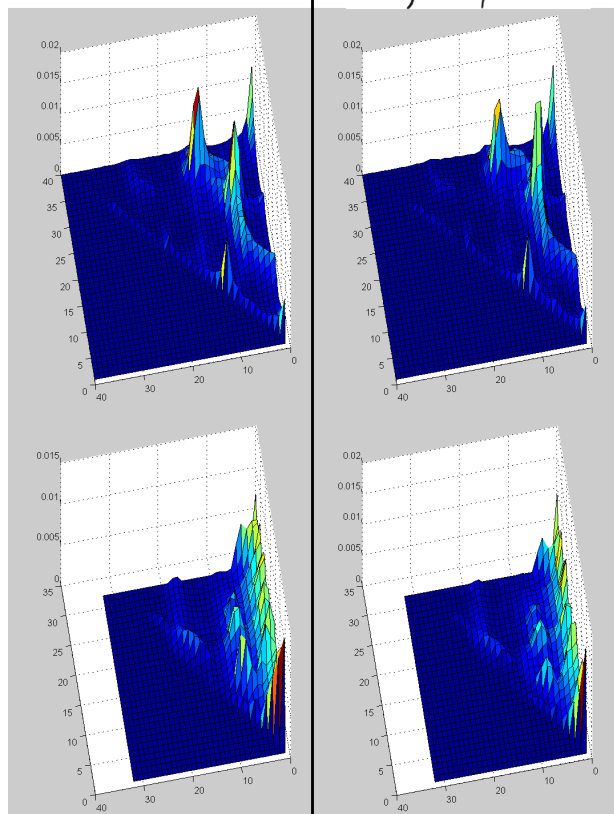


Figure 28. Text samples from the same writer along with skeleton hinge distribution feature surface (middle) and edge hinge combinations feature surface (bottom)

#### 4.1.5 Weighted Skeleton-Hinge Distribution

In our work for Main Body Size Estimation[29], an observation was made in the handwritten document text that characters do not have a single size but vary even in the same text line. In the Weighted Skeleton-hinge distribution, a hypothesis is made that the variations of character size observed in a document image could affect the system's accuracy since they can affect the skeleton hinge distribution. One of the factors affecting the skeleton hinge distribution is the varying character size in a document image. Imagine, for example, a capital "O" and a small "o". The hinge angle on the small "o" is smaller than the hinge angle on the capital "O" at almost any pixel. In this work, a variation of our Main Body estimation technique[29] is utilized to detect local and global Main Body sizes. The ratio of the varying character sizes found locally in a handwritten document image and the document's global character size is considered Weight.

#### 4.1.5.1 Main Body Size And Main Body Map

Usually, in document image processing systems, it is crucial to identify the character size information quickly. The Main Body or core region describes the central part of the text, between the upper baseline and lower baseline, excluding ascenders and descenders (Fig. 29), and it is usually referred to words. This characteristic aims to provide a reference for thresholds and sizes of lines, words and characters as it is directly related to the size of the characters [29].

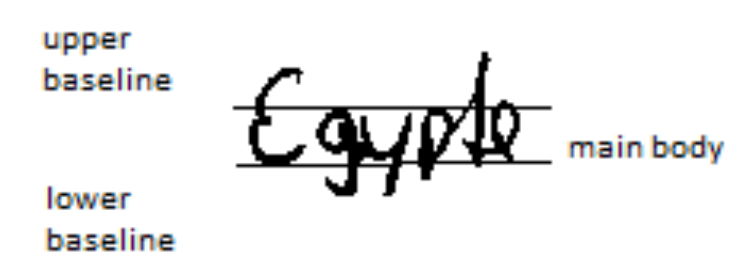


Figure 29. Word main body and baselines

In this work, the Main Body size is referred to small areas of text, usually one or more words, in a part of the text that has a length of  $C$ .

The Main Body Map corresponds to an image, where, when a pixel is on (black pixel) on the document image, the intensity value on the map is the Main Body size value detected in that area of text. For an example of the Main Body Map, see Fig. 30 and 31. Pixels outside of the Main Body area, for example, above the upper baseline and below the lower baseline, are assigned with values equal to the most common Main Body size detected in the document image.

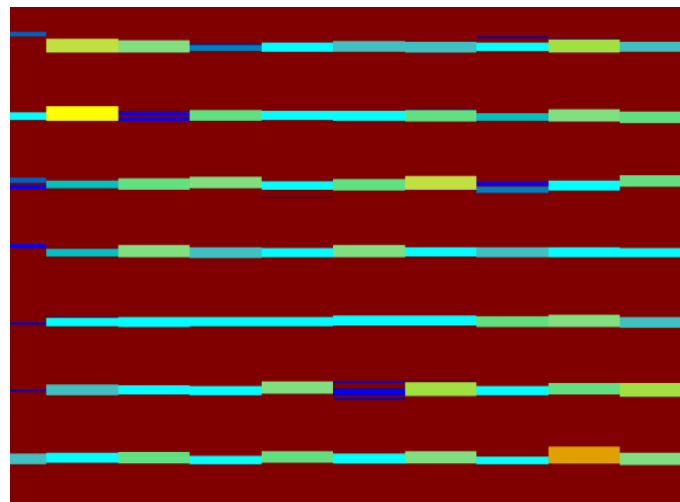


Figure 30. Main Body Map Example



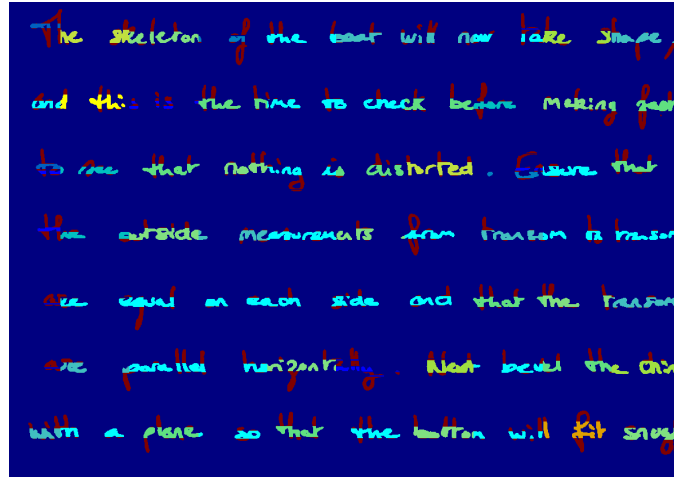


Figure 31. Main Body Map projected on the document image

#### 4.1.5.2 Main Body Size Extraction And Weighted Skeleton Hinge

The Main Body size estimation technique starts by applying a smoothing technique that downsamples the image width while keeping the same height. The technique utilized is a horizontal smoothing procedure that uses the mean value of every  $C$  consecutive pixel. An example of the original text and the smoothed image can be seen in Figures 32 and 33. By observing the resulting image on figures 34 and 35 vertically, it is easily observable that the intensity levels follow a bimodal distribution (Fig 36). Therefore, it is expected that multiple Bimodal distributions will be observed by traversing the new smoothed image vertically. In Bimodal distributions, the external (e.g. top and bottom) modes are expected to take maximum values. For a large enough  $C$ , the external modes correspond to the word baselines (Fig. 29), allowing the estimation of the Main Body Size.

In the proposed MBS estimation methodology, the main idea presented above is used. The smoothed image is traversed vertically, and the bimodal distributions are identified by considering different thresholds. The threshold corresponds to the expected intensity value of the external modes. A range of thresholds is used. On every threshold used, the distances of the external modes detected are considered and stored in a histogram of external mode distances. The distance with the maximum value is considered the most common distance for the selected threshold. This value is stored in the second histogram of threshold distances. Finally, the distance with the max value in the histogram of threshold distances is selected as the most common MBS in the document. Furthermore, the MBS threshold can be found from the maximum frequency value of the MBS from all the histograms of external nodes.

Finally, the Main Body Map is constructed by extracting all the external modes and distances using the MBS threshold. The intensities of the pixels on and between two external modes (upper and lower baselines) are set to the distance value detected for the specific modes. The intensities of the pixel outside of the Main Body area are set to the MBS value.

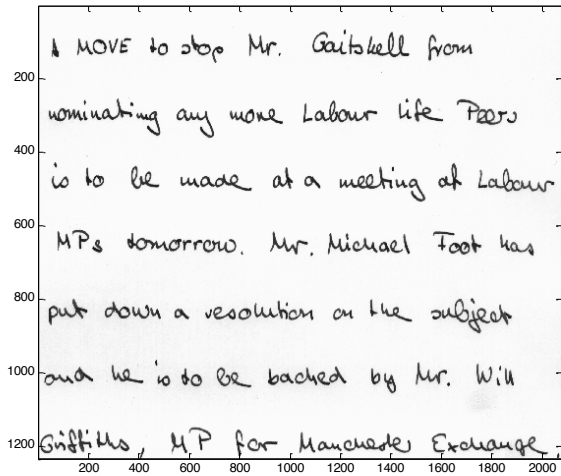


Figure 32. Handwritten document image with a resolution of 1232x2076

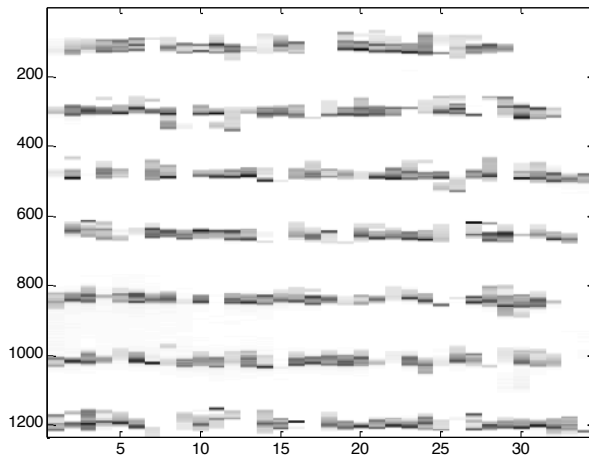


Figure 33. The smoothed version of the document image with the parameter C set to 60 pixels and resolution 1232x34

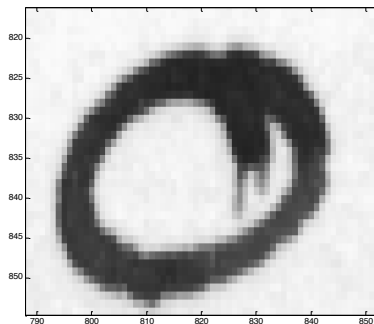


Figure 34. Example of the letter O

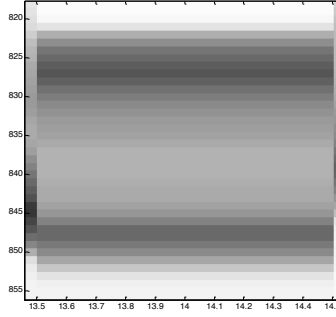


Figure 35. Example of the corresponding smoothed image of the letter O with a height of 35 pixels and width of 1.

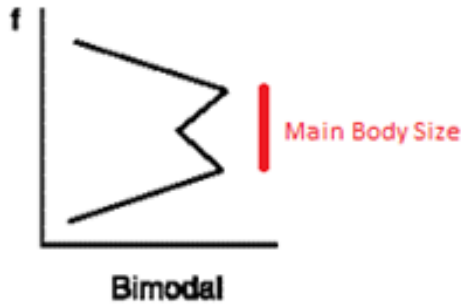


Figure 36. Bimodal distribution

While Skeleton Hinge distribution [28] treats all the skeleton fragments detected in the same way, in the proposed method, the weighted skeleton hinge distribution, the varying size of the text is considered. For example, a word with a large MBS will be treated the same as a word with a smaller MBS in skeleton hinge distribution. In the proposed technique, the Main Body Map information gives different weights on the skeleton hinge fragments detected, according to their central pixel value on the Main Body Map (MBMvalue) and its deviation from the MBS (MBSvalue). The Weight considered is the corresponding value on the Main Body Map divided with the MBS value if the Main Body Map value is lower or equal to the MBS value.

$$Weight(x, y) = \frac{MBMvalue(x, y)}{MBSvalue(x, y)} \quad (1)$$

On the other hand, if the Main Body Map value is greater than the MBS value, then the Weight considered is

$$Weight(x, y) = 1 - \left( \left( \frac{MBMvalue(x, y)}{MBSvalue(x, y)} \right) - 1 \right) \quad (2)$$

#### 4.1.6 Quantized Skeleton Hinge Distribution

Pixel intensity information in Handwritten text is not uniform if we suppose the writing surface is the same for all the writers; the pen is pressed with more power or less power during writing,

depending on the angle, the character, and the written text. In Gray Scale images, we can use the information of pen pressure, denoted as pixel intensity, to augment the skeleton hinge information and prove that those points of pressure provide additional information for the writer's identification.

In this method, the pixel intensity is quantized in  $N$  discrete values. The number of quantizations is used to construct a 3-dimensional matrix with the third direction having a length of  $N$ . Quantized Skeleton Hinge distribution also starts with the image skeleton extraction using a generic skeletonization approach [92]. Then a sliding window technique that uses several window sizes, each quantized in a different number of directions, checks for skeleton line fragments, which emerge from the central window pixel. Finally, their directions and the quantized intensity are measured and stored in triplets. Only skeleton line fragments with  $\phi_1 < \phi_2$  are counted and stored in pairs in a histogram. A joint probability distribution  $p(\phi_1, \phi_2, n)$  is obtained over a large sample of pairs. Finally, the probability distributions acquired by the various sliding window sizes are combined and considered for matching.

#### 4.1.7 Directional Stroke Run Length Hinge Distribution

While skeleton hinge distribution and weighted skeleton hinge distribution perform well, some information might be lost since the skeleton information is used. The same applies to the edge hinge distribution and edge hinge combinations with the edge information.

The main idea behind the Directional Stroke Run Length Hinge Distribution method is to consider all the available information in the document image by utilizing run lengths. To achieve that, all the pixels that are on are considered. Next, a sliding window technique is used with various window sizes, each quantized in directions. On every central pixel that is on the black run lengths, in eight directions are considered. Only the two directions with the most significant run lengths are kept. Next, the direction of the maximum run length is considered. The next pixel is selected by following that direction, and the run lengths of the five directions that emerged from that pixel are considered. The three directions excluded are the opposite direction of the previously selected direction and the two neighbouring directions. This process is repeated by following the pixels found on the largest run lengths from the five directions until the window border is reached. The same technique is applied in the second-largest direction that was initially kept. Finally, the directions of the two run-length directional fragments are measured and stored in pairs—only fragments with  $\phi_1 < \phi_2$  are counted and stored in pairs in a histogram. A joint probability distribution  $p(\phi_1, \phi_2)$  is obtained over a large sample of pairs. The probability distributions, acquired by the various sliding window sizes, are combined and considered for matching. For example, visualizing some of the steps of this technique, see figures 37 to 47.

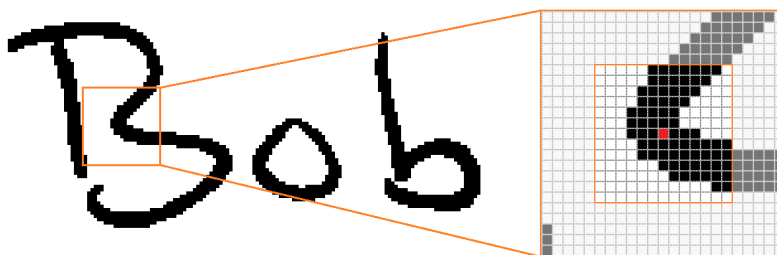


Figure 37. An instance of Stroke Run Length Directional Hinge window of 6 pixels-long fragments with the central pixel selected as starting point.

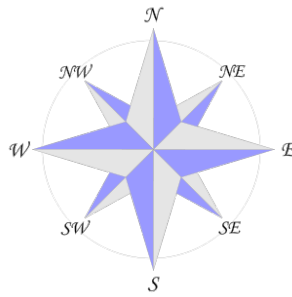


Figure 38. cardinal and intermediate directions will be used to describe run-length directions

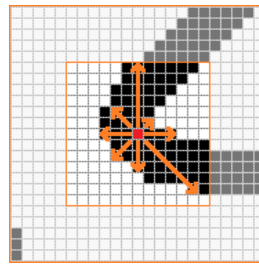


Figure 39. The selected Starting point along with the run lengths in 8 directions with the largest one being 6 pixels length with North direction and the second largest with 5 pixels length on South-East direction

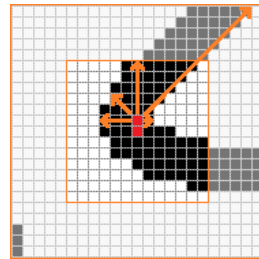


Figure 40. The five directions emerging from the second point along with the run lengths in five directions, with the largest one being in the North-East direction

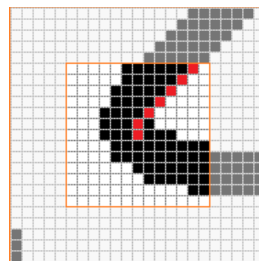


Figure 41. The Largest Run Length is followed until the border is reached

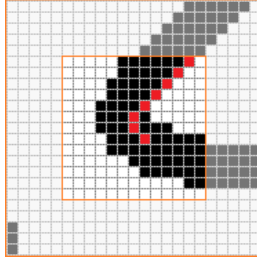


Figure 42. The next pixel is selected in the direction of the second largest direction

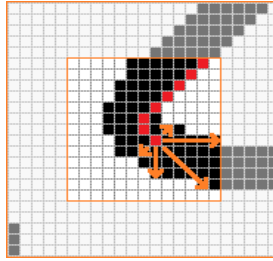


Figure 43. The five directions emerging from the first point on the second-largest direction along with the run lengths in five directions, with the largest one being in the East direction

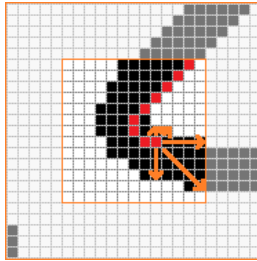


Figure 44. The five directions are emerging from the second point on the second-largest direction and the run lengths in five directions with two directions of equal length of four pixels. The East direction is selected since it was also the direction selected in the previous step.

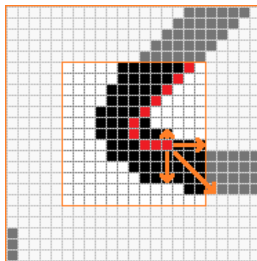


Figure 45. The five directions emerging from the third point on the second-largest direction along with the run lengths in five directions, with the largest one being in the South East direction

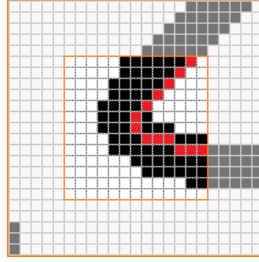


Figure 46. The Largest Run Length is followed until the border is reached

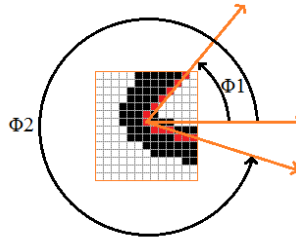


Figure 47. Final Stroke Run Length Directional Hinge with six pixels-long fragments

#### 4.1.8 Run Length Directional Skeleton Hinge Distribution

This method proceeds with the same steps as the Run Length Directional Hinge Distribution, with the only difference being that starting points are located on the image skeleton. First, the image skeleton is extracted using a generic skeletonization approach [92]. All the other pixels are not considered starting points but are considered to locate the most significant run lengths. Next, the directions of the two run-length directional fragments are measured and stored in pairs—only fragments with  $\phi_1 < \phi_2$  are counted and stored in pairs in a histogram. A joint probability distribution  $p(\phi_1, \phi_2)$  is obtained over a large sample of pairs. Finally, the probability distributions acquired by the various sliding window sizes are combined and considered for matching.

#### 4.1.9 Edge-Skeleton-Hinge Combinations

An attempt was made to fill the entire feature space with information on the Edge-Skeleton Hinge Combinations method. All the feature spaces of the previous techniques have one thing in common: the bottom left part of the feature space and the diagonal line from top left to bottom right is empty, which is due because the directions are considered only when  $\phi_1 < \phi_2$ . For example, see Fig. 48

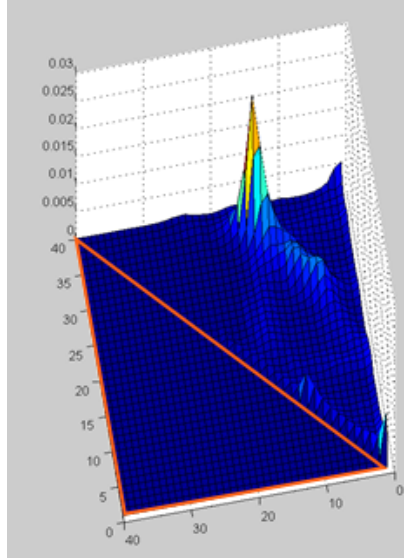


Figure 48. Skeleton-Hinge feature with the area denoted with the triangle being empty

To achieve that, both features, the Skeleton Hinge and the Edge hinge, were considered. The skeleton Hinge feature space was saved in the upper right side of the feature space using the probability distribution  $P_s(\Phi_1, \Phi_2)$ , while the Edge Hinge feature was saved in the bottom left side using an inverse probability distribution  $P_e(\Phi_2, \Phi_1)$ . In Figures 49 and 50, examples from the test set and the train set are presented.

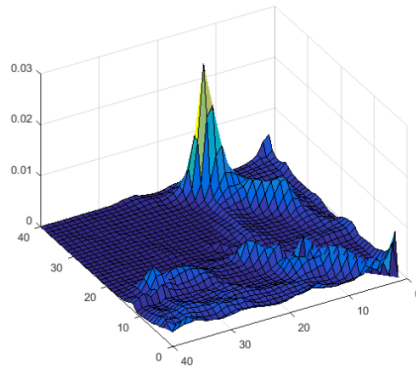


Figure 49. Feature spaces from the Edge-Skeleton Hinge Combinations on the Test sample



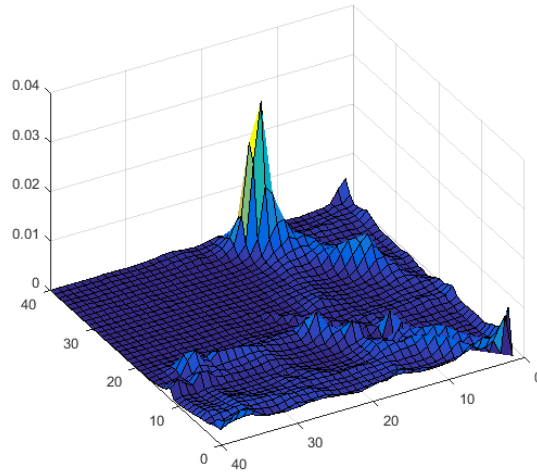


Figure 50. Feature spaces from the Edge-Skeleton Hinge Combinations on Train sample from the same writer.

In the second variation of this technique, an attempt was made to also fill the diagonal line from top left to bottom right. In order to achieve that, we used  $\Phi$  as the difference of  $\Phi_2$  from  $\Phi_1$  and the probability distribution  $Pd(\Phi, \Phi)$

$$\Phi = \Phi_2 - \Phi_1. \quad (5)$$

## 4.2 Model-Based Features

In the Model-Based approach used in the works [25], [34], it is assumed that each writer produces a recognizable set of writer specific character shapes or allographs which happens due to schooling and personal preferences. Therefore, the core idea reflected in the above statement implies that a histogram of used allographs can characterize each writer. However, it is not feasible to have a predefined list of allographs. Instead, training is needed to automatically generate a codebook, which sufficiently captures allograph information from handwriting samples.

The approach used in this work relies on a codebook of models of graphemes. Graphemes are small strokes of handwriting, which are extracted by applying a robust segmentation algorithm on a handwritten image. It should be mentioned that there is a distinction between graphemes and the fragments used in the statistical methods because of the different algorithms in use.

In Schomaker et al. [34], a codebook of graphemes is generated by training a Kohonen SOFM [93] on a large number of grapheme contours. The produced codebook is later used to construct feature vectors.

The process used to create feature vectors from the codebook is quite simple: From each text image, all graphemes are extracted and matched to the grapheme models of the codebook. Euclidean distance between the grapheme contours is used for the matching process. For each grapheme model in the codebook, every successful match is counted. The result is a histogram of graphemes, which characterize the writer and also identify him.

A limitation in this approach is the long training time of Kohonen SOFM. As reported in [34], a training time of up to 122 hours can be required. Besides that, Kohonem SOFM may get stuck in local minima.

Van Der Maaten et al. [25] proposed using random selection to create graphemes rather than using Kohonem SOFM. In this method, no time-consuming training is performed, overcoming the time limitation. Instead of training, a random number of graphemes are drawn from the large set of graphemes.

When combined with the edge-hinge feature, both approaches achieved an identification performance of 97% on the Firemaker DB for 150 distinct writers and a codebook of 400 graphemes.

Here, an improvement was attempted, using a different approach on the codebook generation, by only considering closed areas of the characters. Character closed areas are the least affected by writer slant, very important as slant is a characteristic of the writer that can affect the skeleton hinge distribution.

By combining skeleton hinge distribution with a codebook of graphemes only generated by character closed areas, it was expected to be an ideal way of securing skeleton hinge distribution against forge attempts. A forge attempt can be made by merely changing the slant. However, the results of this approach were not the expected ones.

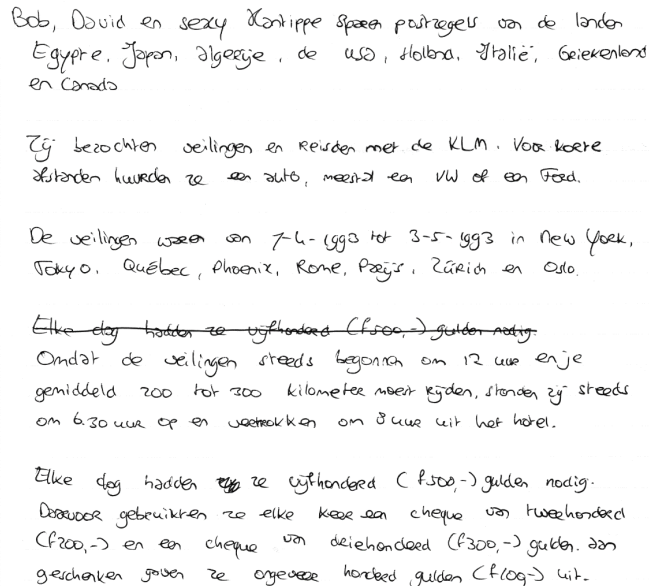
## 5. Main Body And Text Localization

### 5.1 Introduction

In order to validate or dismiss two of our assumptions, and more specifically, the third and fourth assumptions, some preprocessing techniques were developed to facilitate us with this validation.

Firstly, for the third assumption, regarding the effect of Main Body variance in the accuracy of writer identification, two techniques appropriate to detect the Main Body size were developed [29]. Only one was used for writer identification from the two main body size estimation techniques due to its speed and the lower estimation error. Directional Features are susceptible to the Main Body size variance since the angle measured will be narrower in smaller characters and wider in bigger characters. Our approach to validate or dismiss this assumption consists of measuring the global Main Body size of a document and local Main Body size on the word level and use their ratio as the weight for our feature extraction technique. To the best of our knowledge, there is no other paper in the literature specific to Main Body size detection other than [29].

For the fourth assumption, regarding the effect of noise produced by the writer in the accuracy of writer identification, a variation of a technique used for text localization [94] is appropriate to localize only pure text using some rules and dismiss all the noise produced by the writer. This kind of noise usually consists of the writer attempt to erase with ink what he has written by mistake or more minor ink stains that could be regarded as salt and pepper noise. For example, see Fig. 51.



Bob, David en sexy Kontippe speen postzegels van de landen  
Egypte, Japan, Algerije, de us, Holbra, Italië, Geiekenland  
en Canada

Zij bezochten veilingen en reisden met de KLM. Voor korte  
afstanden huurden ze een auto, meestal een VW of een Ford.

De veilingen waren van 7-4-1993 tot 3-5-1993 in New York,  
Tokyo, Quebec, Phoenix, Rome, Praag, Zürich en Oslo.

~~Elke dag hadden ze vijfhonderd (f500,-) gulden nodig.~~  
Omdat de veilingen steeds begonnen om 12 uur en je  
gemiddeld 200 tot 300 kilometer moet rijden, stonden zij steeds  
om 6.30 uur op en vertrokken om 8 uur uit het hotel.

Elke dag hadden ~~zij~~ ze vijfhonderd (f500,-) gulden nodig.  
Daarvoor gebruikten ze elke keer een cheque van tweehonderd  
(f200,-) en een cheque van driehonderd (f300,-) gulden. Aan  
gechenken gaven ze ongeveer honderd gulden (f100,-) uit.

Figure 51. Writers attempt to erase with ink what he has written by mistake

### 5.2 Main Body Size Estimation

#### 5.2.1 First Technique

Our first technique, shown briefly in Fig.52 and analyzed in this section, estimates the average main body of words in a scanned document. Although it has some similarities with [72], it is not that complex; it does not require line segmentation nor image binarisation. Moreover, the

technique is applied to grey level images, although the experimental results prove that if the image is binarised and cleaned from extra noise and converted to grey level, the results are improved.

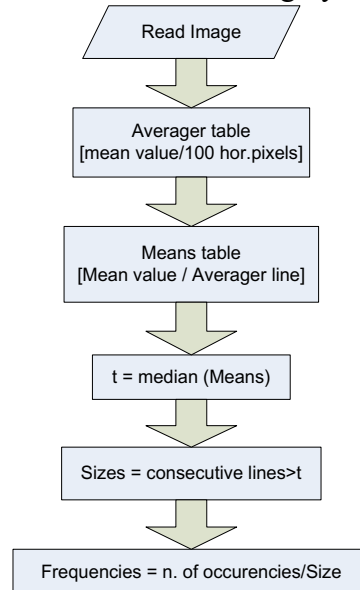


Figure 52. The proposed Main Body Size Extraction methodology.

First, the average pixel value is calculated for every  $N$  pixel in each pixel line of the image.  $N$  can be any value. It is only essential for the skew angle of the page that it can handle. The smaller the  $N$ , the biggest the skew angle it handles. However, since this work does not emphasize that, for the results presented here,  $N=100$  was chosen. The results are saved in the Averager table with size  $H \times [W/100]$ , where  $H$  is the height and  $W$  is the image's width.

Next, the table Means is created of size  $H \times 1$ , where its elements are the average values of the corresponding lines of the Averager matrix. Then the threshold  $T$  is set as the median value of matrix Means. By this threshold, we set to zero the values of Means smaller than  $T$  while we count the consecutive lines with a value larger than  $T$ . Next, the consecutive line sizes are considered as Main Body size occurrences. The occurrences for each size are also counted and saved as Frequencies. Finally, the more frequent Main Body size in Frequencies is considered as Main Body size.

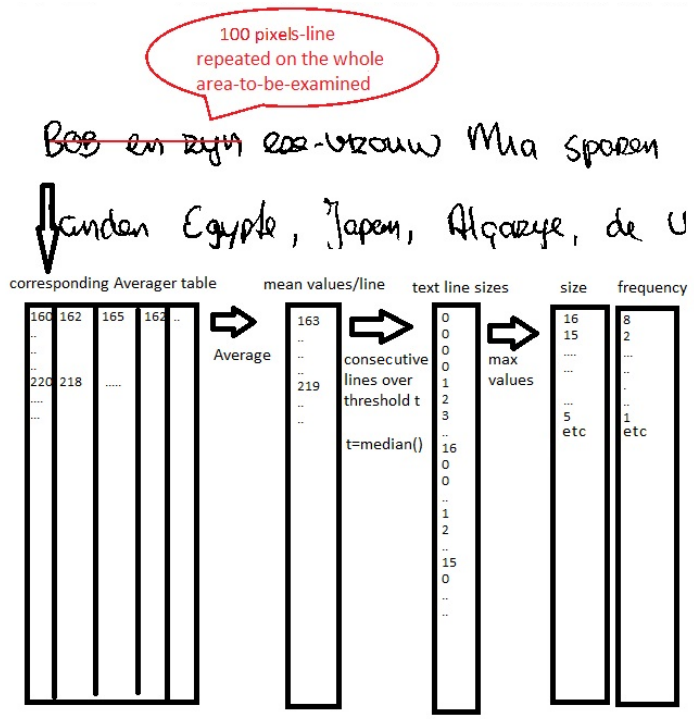


Figure 53. Schematic presentation of the technique through example

In Fig. 53, the technique is presented through an example. This technique does not require binarisation. Moreover, it can give more information if different main body sizes are present on the same page.

### 5.2.2 Second Technique

This technique, developed by Vassilios Veras, a co-author on [29], estimates the baselines of the text in a document page. Initially, the document is binarised. Then, the Connected Components (CCs) of the document are detected for the 8-pixel neighbourhood. Finally, all CCs bigger than 30000 pixels and smaller than 10 pixels are removed, that is, a large area, e.g. scan noise or figures and tiny, noisy areas or accents, respectively.



Figure 54. Vertical dilate.

Then vertical dilate is applied to identify the horizontal borders of the text area (left-right), and if the text consists of text columns, this is necessary since, in the case of the text columns, each column is treated separately. After the vertical dilate the columns of text form a big connected area (Fig.54). Consequently, CCs are again detected, and now only those bigger than 10000 pixels are kept. Finally, a vertical histogram is taken, and those pixel columns with black pixels more than 75% of the average are marked as text and the others as background (Fig.55).

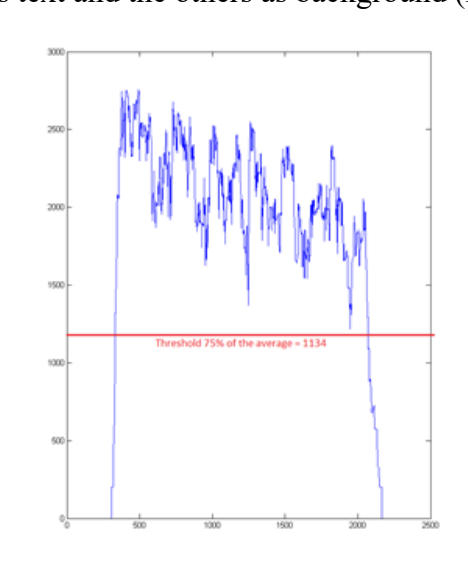


Figure 55. Vertical text localization.

Then the document is scanned from left to right, and the total number of text columns is identified. A similar procedure is followed for each text column, this time with a horizontal dilate (Fig.57). Next, the text lines are detected with their respective start and end indexes in the document. In order to detect the Main Body size, the pixel row must contain 170% of the average pixel rows

(Fig.58); This ensures that the beginning and the end of the main body will be detected, without including the ascenders and the descenders. Finally, the average baselines are calculated and returned as showed in the original document (Fig. 59). The technique is presented in Fig.56.

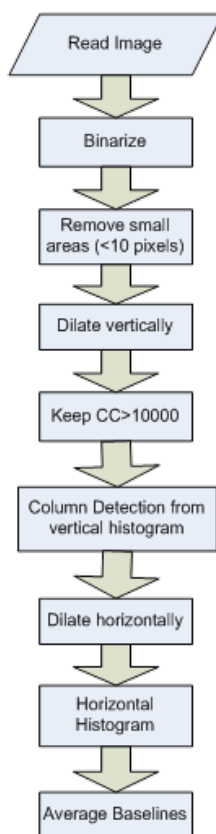


Figure 56. The second technique

Bob en zijn ex-vrouw Mia speelden  
puzzels van de landen Egypte,  
Japan, Algerije, de USA, Holland,  
Italië en Frankrijk. Zij bezochten  
verre landen en reisden met de KLM.  
Voor korte afstanden huurden ze  
een auto, meestal een Fiat of  
VW, waarvoor ze met een  
cheque in euro's (€) betaalden.  
Ze stonden elke week om 6.30 uur  
op en vertrokken daarna  
vroeggestaan uit het hotel,  
waarvoor ze ongeveer honderd  
euro (€100,-) per nacht

Figure 57. Horizontal dilate.

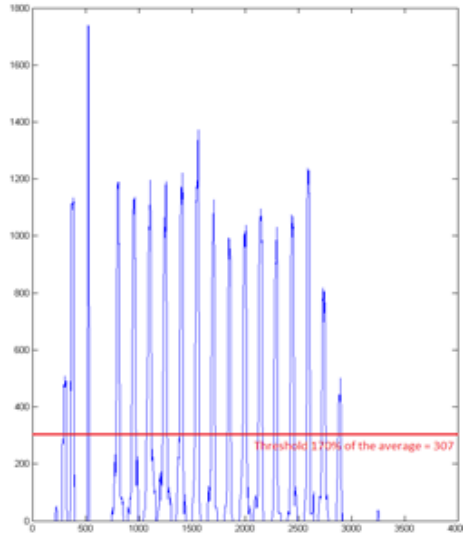


Figure 58. Horizontal text localization.

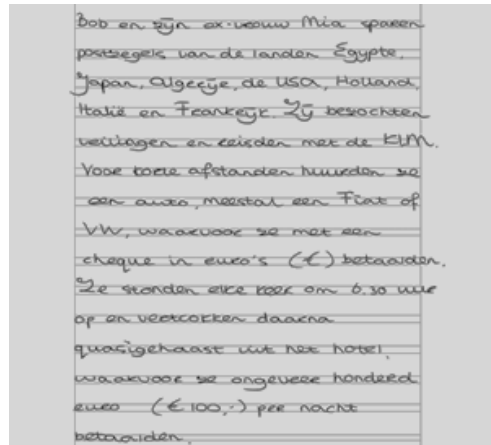


Figure 59. Result with upper and lower baselines visible

### 5.2.3 Experimental Results

Evaluating a technique that estimates the text Main Body size is not easy, primarily when referring to the handwritten text. Therefore, the TrigraphSlant data set [95] containing images of handwriting produced under natural and forced slant conditions were used. It includes 190 images from 47 persons. In addition, 30 images of natural writing by different writers were used.

In order to create ground truth data, the height of 10 'o' of each image was measured, and the mean value was considered. It took us by surprise that even on the same document image, written by the same person, differences of more than 10 pixels were found.

In table 1, the mean estimated Main Body size for five writers (D00X), along with the results for 4 document images of the same writer (D00X-1, D00X-2, D00X-3, D00X-4). It is obvious how the size changes, even for the same writer. Only the first document image (D00X-1) of each writer for X between 1 and 30 was used in our experiments.



Since, as explained, it is difficult to have exact results, in table 2, the average error deviation between the estimated values and the ones detected by the two techniques is given. Moreover, to give more objective results, in the same table, the average error deviation between the actual values and the ones detected by the two techniques over a collection of 10 printed images that includes font sizes between 8 and 24 pts is also given.

Table 1. Examples of Main Body size estimation

<i>Document Code</i>	<i>Image</i>	<i>Estimated Mean Main Body Size (pixels)</i>
D001-1-An		34,8
D001-2-Bn		35,2
D001-3-Bl		31,6
D001-4-Br		31,6
D002-1-An		33,6
D002-2-Bn		27,4
D002-3-Bl		37,2
D002-4-Br		27,2
D003-1-An		34,2
D003-2-Bn		33,4
D003-3-Br		30,8
D003-4-Bl		33,4
D004-1-An		29,2
D004-2-Bn		29,2
D004-3-Br		32,8
D004-4-Bl		34,2
D005-1-An		34,6
D005-2-Bn		34,2
D005-3-Br		28
D005-4-Bl		33,4

Table 2. Experimental Results

<i>Technique</i>	<i>Average error deviation (pixels) on Trigraph</i>	<i>Average error deviation (pixels) on printed DB</i>
first	2.17	0.67
second	4.96	1.05

## 5.3 Text Localization

### 5.3.1 System Overview

The proposed method, developed by Ergina Kavalieratou and Pilar Gomez-Gil, co-authors on [94], takes advantage of two facts: a) a text should contrast with its background in order to be readable; b) a text follows some regularity in any language. Figure 60 shows the main steps of this method. First, an RGB image is transformed into a grayscale image using the formula [96]:

$$gray = 0.2989 * R + 0.5870 * G + 0.1140 * B \quad (3)$$

Where R, G, B correspond to the colour of the pixel, respectively. This image is binarised for using various thresholds, which is defined as:

$$threshold = minimumI + k * STEP \quad (4)$$

Where minimumI corresponds to the minimum intensity of the grayscale image and STEP is a small value. In the experimental results reported here, STEP values go from 1 to 7. The k parameter considers values from 1 up to (maximumI - minimumI)/STEP in order to cover with various thresholds all the range between the minimum (minimumI) and the maximum (maximumI) of the grayscale image. A binary image and its reversed one are built, using as threshold all the multiples of a specific STEP. The reverse image is also used since it cannot be known if the foreground is lighter or darker.

Using all possible black and white images, all possible contrasts should be included for a small step. After this, each image is examined in detail for the existence of several constraints that the parts of images corresponding to texts are expected to accomplish:

1. Similar colours between the text parts or dissimilarity less than 10% are expected.
2. Within a text region, the dissimilarity in colour should remain less than 10%.
3. Areas with either size less than 5 pixels are not considered.
4. The parts of the text, usually characters, are expected to have a similar width, with a maximum deviation of 10%. A difference of up to 50% is allowed in height to include words with uppercase and lowercase letters.
5. Neighbour text parts are expected to have similar areas with a deviation of a maximum of 30% due to the difference between characters and uppercase/lowercase letters.
6. The parts of the same text square are expected to have a horizontal distance of a maximum 3xMB and a vertical distance of one MB, where MB is a rough approach of the mean character size.

As it is mentioned in [78]: By mean width of the character, we consider the width of characters such as a, b, c, d etc., excluding the characters i, l, j, m, w that are either too narrow (i, j, l), or too broad (m, w). ... Although the character width differs between characters and writers, a rough estimation of the mean width could be made by accepting that excluding the ascenders and descenders the characters with mean width (as defined above), present width equal to their height. Thus, MB is estimated as the CCs height; rules 4, 5 and 6 derive from the above definition.

CCs of every binary image is extracted, and several properties are calculated:

- The centroids of the CCs.
- The minimum, maximum and mean intensity of the corresponding area in the grayscale image.
- The area of each CC.

- The bounding boxes of each CC. along with the coordinates of the upper left corner and their width and height.
- The main body, as the height of the CC.

Then, for each pair of CCs and using these properties, the rules described above are applied, respectively:

1. The mean intensity of the two CCs is expected not to differ more than 10%.
2. The minimum and maximum intensity of each CC is expected not to differ more than 10%.
3. The CCs with an area less than 10 pixels or Bounding Box width or height less than 5 pixels are eliminated.
4. Both bounding box heights and widths are required not to differ more than 10%.
5. The areas of the CCs are expected not to differ more than 30%
6. The  $x$  coordinates of CCs centroids are expected to be situated within 3MB and the  $y$  coordinates within one MB.

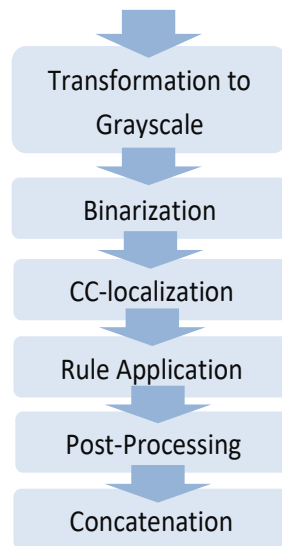


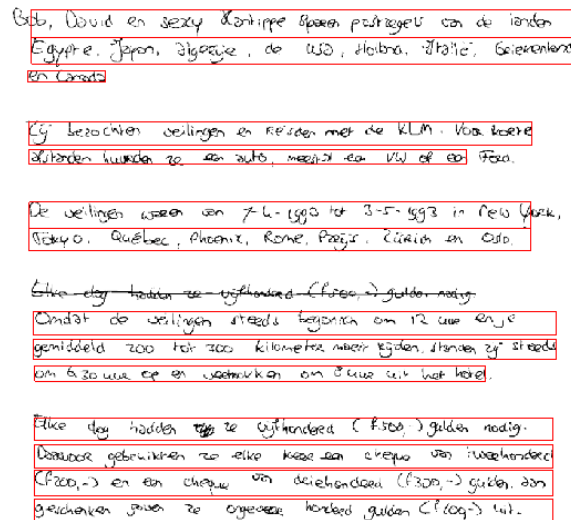
*Figure 60. The tasks of the proposed system*

A pair of CCs that successfully pass the above constraints is considered part of the same group. Then, the procedure is repeated for the reverse image. As a result, from each image, several areas are extracted as possible text areas. Considering that natural scenes can include all grayscale tones from 0 to 255 (not always), some dozens of binary images are considered, and the extracted areas could be up to hundreds. However, since they are black and white images, the processing is fast. Thus, the extracted areas are unified if the following rule holds:  
 IF the mean value of the  $y$ -coordinates of an area is included in the  $y$ -coordinates of another area AND (their areas are either overlapped, OR they are not located more than one MB apart, horizontally.)

At this point, our system presented a recall >70%, which is very high compared to the results of other systems of the competition but very low precision. This is the reason that a post-processing stage was included in the system. In this post-processing stage, every single part of the image is analyzed in order to confirm that it includes text. Thus, it includes the following procedures:

- First, the image is cleaned on all sides, above, below, left and right by pixel lines that include entirely white or entirely black pixels.
- Then, if horizontal pixels lines include only white or only black pixels, the image is split into horizontal text lines, limited by these pixel lines.
- Finally, it is checked if there are entire columns with only white or black pixels expected to separate characters.

Once the post-processing is done, a concatenation procedure is applied to unify the overlapped parts of the image.



Bob, David en sexy koninkje spelen potageu van de landen  
Egypte, Japan, Griekenland, de VS, Holbro, Italië, Griekenland  
en Canada

Eg bezochten vestingen en reisden met de KLM. Via boere  
stribden kwamen ze een auto, meestal een VW of een Ford.

De vestingen waren van 7-6-1992 tot 3-5-1993 in New York,  
Stokholm, Quebec, Phoenix, Rome, Praag, Zürich en Oslo.

Stroefdag hadden ze vijfhonderd (F500,-) gulden nodig.  
Omdat de vestingen steeds bereikbaar om 12 uur en de  
gemiddeld 200 tot 300 kilometer meer rijden, stonden zij steeds  
om 5.30 uur op en waarmaken om 12 uur uit het hotel.

Elke dag hadden zij ze vijfhonderd (F500,-) gulden nodig.  
Daarvoor gebruikten ze elke keer een cheque van vijfhonderd  
(F500,-) en een cheque van driehonderd (F300,-) gulden, dan  
beschikten zij over de ongeveer honderd gulden (F100,-) uit.

Figure 61. Text localization result example of the document from Figure 51.

Jo, David en sexy Konijpe sporen passagiers van de landen  
Egypte, Japan, Algerije, de uss, Holbra, Italië, Griekenland  
en Canada

Zij bezochten veilingen en reisden met de KLM. Voor boete  
sluitenden huurden zo een auto, meestal een VW of een

De veilingen waren van 7-4-1993 tot 3-5-1993 in New York  
Tokyo, Quebec, Phoenix, Rome, Parijs, Zürich en Oslo.

Omdat de veilingen steeds begonnen om 12 uur en je  
gemiddeld 200 tot 300 kilometer meer rijden, stonden zij steeds  
om 6:30 uur op en waerkken om 8 uur uit het hotel

Elke dag hadden zij te vijfhonderd (f500,-) gulden nodig.  
Daarvoor gebruikten zo elke keer een cheque van tweehonderd  
(f200,-) en een cheque van driehonderd (f300,-) gulden. Aan  
geschonken gaven zo ongeveer honderd gulden (f100,-) uit.

Figure 62. Final image after text localization, on the document from Figure 51.

### 5.3.2 Experimental Results

For evaluating the proposed procedure, the dataset of ICDAR 2011 Robust Reading Competition Challenge 2: Reading Text in Scene Images [89] was used. The final dataset consisted of 485 images containing text in various colours and fonts on many different backgrounds and orientations. A comparison of our results with other techniques is shown in Table 3. Furthermore, after filtering the document images with this technique and using the Skeleton Hinge distribution for feature extraction, experimental results for the writer identification task can be found in chapter 6.

Table 3. Comparative results with the dataset of ICDAR 2011 Robust Reading Competition Challenge 2: Reading Text in Scene Images [96].

Method	Recall	Precision	Harmonic Mean
technique 1	62.47	82.98	71.28
technique 2	58.09	67.22	62.32
technique 3	57.68	66.97	61.98
technique 4	52.54	68.93	59.63
technique 5	53.52	63.52	58.09
technique 6	50.07	62.97	55.78
technique 7	44.57	59.67	51.03
technique 8	38.32	35.01	36.59
technique 9	25.96	50.05	34.19
<b>Proposed Technique</b>	<b>77.08</b>	<b>57.15</b>	<b>65.63</b>

## 6. Writer Identification Experimental Results

### 6.1 Data Sets

#### 6.1.1 Firemaker DB

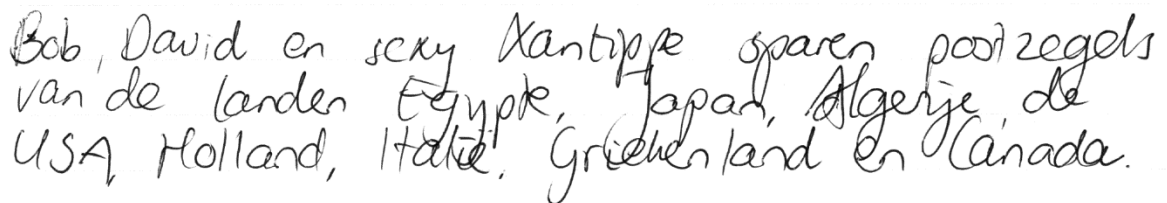
One of the datasets used to evaluate the feature extraction techniques presented in this work was the Firemaker Database [14]. This data set was used to directly compare the achieved results with the reported ones by the other methods.

The Firemaker is a database of handwritten pages from 250 writers, including four pages per writer.

- Page 1 contains a copied text in natural writing style
- Page 2 contains a copied text in Upper-case text
- Page 3 contains copied forged text. The writers here try to impersonate another writer.
- Page 4 contains a self-generated description of a cartoon image in free writing style. On this last page, the text content and the amount of written ink varies considerably per writer.

All pages in Firemaker Database were scanned at 300-dpi grayscale. The text that was asked to be copied was specially designed in forensic praxis to cover many different alphabet letters. In our experiments, only pages 1 and 4 were used. Page 1 was used as a training set. While page 4 was used as a test set.

proefnr:	geb.dat:	166175	man	links
(in te vullen door NICI)	huisnr:	17	Vrouw	rechts $\alpha$
NICI datacollectie 1999		Tekst1: Bob en David ... (f100,-) uit.		



Bob, David en sexy Kantippe sparen postzegels van de landen Egypte, Japan, Algerije, de USA, Holland, Italië, Griekenland en Canada.

Figure 63. Part of a Document image from Firemaker DB

#### 6.1.2 ICDAR 2017 Writer Identification Competition

Additional experiments were performed on the Skeleton Hinge Distribution feature using the ICDAR 2017 writer identification competition [15] dataset. The dataset used for this competition consists of 3600 document images, which 720 different writers have written. Each writer has contributed five documents. The performance was evaluated using ScriptNet, the competition platform which can output the mean average precision (map) and top 1 performance.

## 6.2 Experiments

### 6.2.1 Skeleton Hinge Distribution

Various experiments were performed, using combinations of several parameters, e.g. window sizes and matching classifiers. However, it is hard to compare our results with results reported on other papers because of the variation in the data sets. Therefore, our results will be only comparable to methods that used the same dataset.

Furthermore, even on the same dataset, results can have a significant variation. For example, some methodologies only used a fragment of the entire dataset without mentioning which one exactly. Also, there are differences in train and test sets. Even a slight change in these sets can change the entire outcome.

For the training (Extract Skeleton Hinge training Features), only page 1 from the Firemaker DB was used. Each page was binarised, and the skeleton was extracted using Matlab. The used procedure is the one described in the previous section for skeleton hinge distribution.

The training procedure was fast, about 250 seconds on a laptop i7 2.5Ghz pc, and in comparison to the edge hinge distribution, about 35% faster. On the same machine, the edge-hinge distribution train took 384 seconds to complete.

To extract Skeleton Hinge test Features, only page 4 was used from the Firemaker DB. The testing process used the same procedure as the training process.

The test procedure was faster than training due to the variations in text sizes on page 4. Testing took around 200 seconds on a laptop i7 2.5 GHz. Edge hinge distribution time was about 270 seconds. An improvement of about 35% can be observed here, too.

Different matching techniques were considered for writer identification—maximum accuracy achieved with the Nearest Neighbour classifier with Manhattan distance. Euclidean and chi-square distances were also considered for classifying, but they performed worse than Manhattan distance. KNN classifier was also considered with k 1.

Furthermore, clustering techniques, like K-means and Agglomerative Hierarchical Cluster Trees, and machine learning techniques, like SVM, were considered.

#### 6.2.1.1 Skeleton Hinge Features With The Nearest Neighbour Classifier On Firemaker DB.

Skeleton Hinge Distribution Feature identification results are presented in Table 4. These experiments used the entire data set of 250 writers. Like the edge-hinge combinations method, a combination of fragment lengths, i.e. window sizes were used. Furthermore, for the nearest neighbour classifier Manhattan, Euclidian and chi-square distances were used. Our top result is identification accuracy of 90.8 % for a combination of fragment lengths of 5- and 9-pixel length window and Manhattan distance.

Table 4. Skeleton Hinge Distribution Accuracy (Percentage) on Firemaker DB

Fragment Length	Skeleton Hinge Distribution Accuracy (Percentage)		
	<i>Manhattan Distance</i>	<i>Euclidian Distance</i>	<i>Chi-square Distance</i>
3	80%	72%	53.2%
5	89.6%	77.2%	66%
7	90%	81.6%	69.6%
9	88%	85.2%	76%
3 , 5	85.2%	75.2%	58.4%
3 , 7	85.6%	75.6%	55.2%
3 , 9	86%	74.8%	53.2%
5 , 7	90%	78.8%	64.4%
5 , 9	<b>90.8%</b>	78.8%	67.2%
7 , 9	90%	83.2%	73.6%
3 , 5 , 7	86.8%	76.8%	60%
3 , 7 , 9	89.6%	76.8%	55.6%
5 , 7 , 9	90%	79.2%	68.8%
3 , 5 , 7 , 9	89.6%	76.8%	60.4%

#### 6.2.1.2 Skeleton Hinge Features With The Nearest Neighbour Classifier On ICDAR 2017

Skeleton Hinge Distribution Feature identification results on ICDAR 2017 dataset are presented in Table 5. These experiments used the entire data set of 3600 document images, which 720 different writers have written. Like the edge-hinge combinations method, a combination of fragment lengths, i.e. window sizes were used. In addition, for the nearest neighbour classifier, Manhattan distances were used. Our top result is identification accuracy of 68.44% with a mean average precision (map) of 47.02% for a combination of fragment lengths of 3-5-7 and a 9-pixel length window. Finally, in Table 6, an overview of results reported in [15] compared to our results is presented.



Table 5. Skeleton Hinge Distribution Accuracy (Percentage) on ICDAR 2017 writer identification competition Data Set

<b>Fragment Length</b>	<b><i>WI-map</i></b>	<b><i>WI-precision</i></b>
3	40.57%	60.83%
5	44.80%	66%
7	43.96%	64.63%
9	40.99%	61.41%
3 , 5	44.50%	65.58%
3 , 7	46.20%	67.33%
3 , 9	46.33%	67.52%
5 , 7	45.98%	67.22%
5 , 9	46.34%	67.66%
7 , 9	43.73%	64.33%
3 , 5 , 7	46.34%	67.75%
3 , 7 , 9	46.92%	68.36%
5 , 7 , 9	46.11%	67.33%
3 , 5 , 7 , 9	<b>47.02%</b>	<b>68.44%</b>

Table 6. Skeleton Hinge Distribution Accuracy (Percentage) on ICDAR 2017 writer identification competition Data Set as reported in [15]

<b>Method</b>	<b><i>WI-map</i></b>	<b><i>WI-precision</i></b>
Skeleton Hinge	<b>47.02%</b>	<b>68.44%</b>
Barcelona	45.9%	67%
Fribourg	30.7%	47.8%
Groningen	54.2%	76.1%
Hamburg	46.9%	67.1%
Tebessa I	52.5%	74.4%
Tebessa II	55.6%	55.6%

### 6.2.1.3 Skeleton Hinge Features With K-means And Hierarchical Cluster Tree Identification Results.

An attempt was made to identify writers using the k-means algorithm and partitioning the collection into clusters on Firemaker DB. The entire collection consisted of 250 writers with two pages per writer, one page in training data, and one page in test data. Skeleton hinge distribution features were extracted from 500 pages and partitioned into 250 clusters. Standard K-means technique was used, as well as Kmeans with different distance parameters were explored. Only

clusters that included both pages from each writer were considered as correctly identified. Identification accuracy reached 66.8% using 3,5,7,9 skeleton hinge distribution combinations.

Furthermore, experiments of clustering the 500 pages using an Agglomerative hierarchical cluster tree were made using two parameters, Agglomerative clusters from linkages and Agglomerative clusters directly from data. Only clusters containing both pages from the same writer were considered as correctly identified. Accuracy in both methods reached 63.6% using 3,5,7,9 skeleton hinge distribution combinations.

Skeleton Hinge Distribution Features clustered with K-means and Hierarchical cluster tree identification results are presented in Table 7.

Table 7. K-means and Hierarchical cluster tree identification Results on Firemaker DB

Clustering Method	Parameter	Accuracy
K-means	normal	66.8%
K-means	city block	46.4%
K-means	cosine	66.8%
K-means	correlation	66.8%
Hierarchical Cluster Tree	linkages	63.6%
Hierarchical Cluster Tree	data	63.6%

#### 6.2.1.4 Skeleton Hinge Features With Nearest Neighbor Using KNN Results.

Besides using a simple Euclidean distance measure, the KNN algorithm was used to find the nearest neighbour of every document of the training set in the test set on Firemaker DB. From each set, skeleton hinge distribution combinations with fragment lengths 3,5,7,9 were extracted. Different distance measures were used. In most of them, accuracy reached 76.8%, while with city blocks distance, accuracy reached 89.6%. Skeleton Hinge Features with Nearest Neighbor using KNN results are presented in Table 8.

Table 8. Skeleton Hinge Identification Accuracy using KNN on Firemaker DB

Method(k=1)	Distance	Accuracy
KNN	Chebychev	51.6%
KNN	Minkowski	76.8%
KNN	Cosine	76.8%
KNN	Correlation	76.8%
KNN	Hamming	1.2%
KNN	Seuclidean	0.4%

KNN	Cityblock	89.6%

#### 6.2.1.5 Skeleton Hinge Features With Support Vector Machines Results.

Support vector machines (SVM) were used as well to identify the writer on Firemaker DB. A simple scheme of “one-vs-all” was used in an iterative process. A single document from the training set, consisting of 250 writers, was assigned as known and the rest unknown in each iteration. An SVM was trained using the skeleton hinge distribution combinations with fragment lengths 3,5,7,9 extracted from the training set and the class information assigned to them. Next, a new iteration was used to classify the documents in the test data set, after extracting the skeleton hinge distribution combinations with fragment lengths 3,5,7,9, according to the trained model. Accuracy was 53.6%

SVM with a one-vs-one scheme was also considered but trained only in the first 100 writers. In each iteration, a classifier was trained to distinguish between documents of 2 distinct writers. All the possible non-overlapping combinations were considered. A total of 4950 classifiers were trained. The SVM classifiers were trained using the 3,5,7,9 skeleton hinge distribution combinations from the train set. Next, a new iteration was used to classify the documents in the test set. Every handwritten document was classified using the trained classifiers. Matching is achieved with a voting procedure. The most voted class is assigned to the document. Accuracy for 100 writers achieved 63%. Skeleton Hinge Features with Support Vector Machines results are presented in Table 9.

Table 9. Skeleton Hinge Features with Support Vector Machines results on Firemaker DB.

<b>Scheme</b>	<b>Number of writers</b>	<b>Accuracy</b>
One-vs-all	250	53.6%
One-vs-one	100	63%

### 6.2.2 Codebook of Graphemes And Skeleton Hinge Distribution

In addition, an attempt was made to combine skeleton hinge distribution with a codebook of graphemes method on Firemaker DB. The results of this experiment are presented in Table 10. The model-based methods [25], [34] reported accuracy of up to 97% on 150 writers, using a codebook of size 400 when the results were combined with edge-directional features. Unfortunately, it was impossible to train a codebook of 400 graphemes for 250 writers due to memory issues.

Instead, a codebook of 225 graphemes was trained for 250 writers. Maximum accuracy of 95,6% was reached. It is necessary to mention that the other methods reported 97 % accuracy on 150 writers with a codebook of 400 graphemes. In our case, an experiment was also performed using 150 writers of the data set and a codebook of 225 graphemes. An accuracy of 96% was achieved.

Codebook of Graphemes combined with Skeleton Hinge Distribution feature identification results is presented in Table 10.

Table 10. Skeleton Hinge Distribution Combined with Codebook of Graphemes Method Accuracy (Percentage) on Firemaker DB

Number of Writers	CodeBook Size	Skeleton Hinge Distribution Combined with Codebook of Graphemes Method		
		<i>Manhattan Distance</i>	<i>Euclidian Distance</i>	<i>Chi-square Distance</i>
250	225	95.6%	91.2%	78.8%
150	225	96%	94.7%	86.7%

### 6.2.3 Quantized Skeleton Hinge Distribution

In this section, experiments were performed only for combining fragment lengths 5 and 9 since that combination achieved an accuracy of 90.8% on the Skeleton Hinge Distribution on Firemaker DB. The experiments were performed on 250 writers using Manhattan Distance and quantized in 1,2,3,4,5,9 intensity levels. Quantized Skeleton Hinge Distribution feature identification results are presented in Table 11.

Table 11. Quantized Skeleton Hinge Distribution Accuracy (Percentage) on Firemaker DB

Number Of Quantizations	Quantized Skeleton Hinge Distribution
1	90.8%
2	92%
3	<b>92.4%</b>
4	89.6%
5	91.2%
9	88.4%

### 6.2.4 Weighted Skeleton Hinge

In this section, experiments were performed with combinations of various fragment length sizes (i.e. window sizes) were considered on pages 1 and 4 of the Firemaker DB, conducted on 250 writers using Manhattan Distance. For comparison with previous methods, we included the

results of Edge Hinge Combinations (EHC), as reported in [25] and Skeleton Hinge Distribution (SHD) as reported in [28]. In addition, weighted Skeleton Hinge Distribution (WSHD) features identification results are presented in Table 12.

Table 12. EHC, SHD, WSHD identification Accuracy (Percentage) with Manhattan Distance on Firemaker DB

<b>Fragment Length Combinations</b>	<b>EHC Accuracy (Percentage)</b>	<b>SHD Accuracy (Percentage)</b>	<b>WSHD Accuracy (Percentage)</b>
3	68%	80%	82%
5	70%	89.6%	88.8%
7	70%	90%	90%
9	69%	88%	88.8%
3, 5	77%	85.2%	85.2%
3, 7	77%	85.6%	85.6%
3, 9	79%	86%	86%
5, 7	74%	90%	89.6%
5, 9	77%	<b>90.8%</b>	<b>91.2%</b>
7, 9	72%	90%	89.6%
3, 5, 7	80%	86.8%	87.6%
3, 7, 9	78%	89.6%	89.2%
5, 7, 9	76%	90%	90.8%
3, 5, 7, 9	<b>81%</b>	89.6%	88.4%

### 6.2.5 Run Length Directional Hinge

In this section, experiments were performed with combinations of various fragment length sizes (i.e. window sizes) were considered on pages 1 and 4 of the Firemaker DB, performed on 250 writers using Manhattan Distance. For comparison with previous methods, we included the results of Edge Hinge Combinations (EHC), as reported in [25] and Skeleton Hinge Distribution (SHD) as reported in [28]. In addition, run Length Directional Hinge Distribution (RLDHD) features identification results are presented in Table 13.

Table 13. EHC, SHD, RLDHD identification Accuracy (Percentage) with Manhattan Distance on Firemaker DB

<b>Fragment Length Combinations</b>	<b>EHC Accuracy (Percentage)</b>	<b>SHD Accuracy (Percentage)</b>	<b>RLDHD Accuracy (Percentage)</b>
3	68%	80%	85.2%
5	70%	89.6%	89.2%
7	70%	90%	90.4%
9	69%	88%	<b>91.2%</b>
3, 5	77%	85.2%	88%
3, 7	77%	85.6%	89.2%
3, 9	79%	86%	89.2%
5, 7	74%	90%	89.6%

5 , 9	77%	<b>90.8%</b>	89.2%
7 , 9	72%	90%	90.4%
3 , 5 , 7	80%	86.8%	88.8%
3 , 7 , 9	78%	89.6%	89.2%
5 , 7 , 9	76%	90%	90%
3 , 5 , 7 , 9	<b>81%</b>	89.6%	89.2%

### 6.2.6 Edge Skeleton Hinge Combination

In this section, experiments were performed with combinations of various fragment length sizes (i.e. window sizes) were considered on pages 1 and 4 of the Firemaker DB, conducted on 250 writers using Manhattan Distance. For comparison with previous methods, we included the results of Edge Hinge Combinations (EHC), as reported in [25] and Skeleton Hinge Distribution (SHD) as reported in [28]. Edge Skeleton Hinge Combination (ESHC) features identification results are presented in Table 14

Table 14. EHC, SHD, ESHC identification Accuracy (Percentage) with Manhattan Distance on Firemaker DB

Fragment Length Combinations	EHC Accuracy (Percentage)	SHD Accuracy (Percentage)	ESHC Accuracy (Percentage)
3	68%	80%	79.4%
5	70%	89.6%	89.2%
7	70%	90%	89.6%
9	69%	88%	87.2%
3 , 5	77%	85.2%	84.6%
3 , 7	77%	85.6%	85.2%
3 , 9	79%	86%	85.6%
5 , 7	74%	90%	89.6%
5 , 9	77%	<b>90.8%</b>	<b>90.2%</b>
7 , 9	72%	90%	89.4%
3 , 5 , 7	80%	86.8%	86.8%
3 , 7 , 9	78%	89.6%	89.2%
5 , 7 , 9	76%	90%	89.4%
3 , 5 , 7 , 9	<b>81%</b>	89.6%	89.2%

### 6.2.7 Directional Features Comparison

In this section, a comparison of top identification results reported in the literature on Firemaker DB, and in the sections above for the directional features of Edge Direction Distribution, Edge Hinge Combinations, Skeleton Hinge Distribution, Quantized Skeleton Hinge Distribution, Weighted Skeleton Hinge Distribution, Run Length Directional Hinge Distribution, Quill-Hinge and Junctions are presented in Table 15. Furthermore, a graphical representation of the results on Edge Hinge Combinations, Skeleton Hinge Distribution, Weighted Skeleton Hinge Distribution and Run Length Directional Hinge Distribution on common fragment length combinations is given in Fig. 64

Table 15. EDD, EHC, SHD, QSHD, WSHD, RLDHD, ESHC, and methods from literature identification Accuracy (Percentage) with Manhattan Distance on Firemaker DB

<b>Method</b>	<b>Accuracy Reported</b>
EDD	35%
EHC	68%
SHD	90.8%
QSHD	92.4%
WSHD	91.2%
ESHC	90.2%
RLDHD	91.2%
Edge-Hinge [24]	63%
Codebook of Graphemes combined with Edge-Hinge [34]	97%
Edge-Hinge combinations [25]	81%
Codebook of Graphemes combined with Edge-Hinge Combinations [25]	97%
Contour-Hinge combined with Writer-Specific Grapheme Emission PDF [41]	83%
SDS+SOH [43]	92.4%
Quill-Hinge [26]	86%
Junclets [30]	80.6%
Junclets+Hinge [30]	89.8%
BW-LBC [51]	94.4%
CLGP [52]	97.6%
Dissimilarity GMM (DGMM) [54]	97.98%
GR-RNN [20]	98.8%

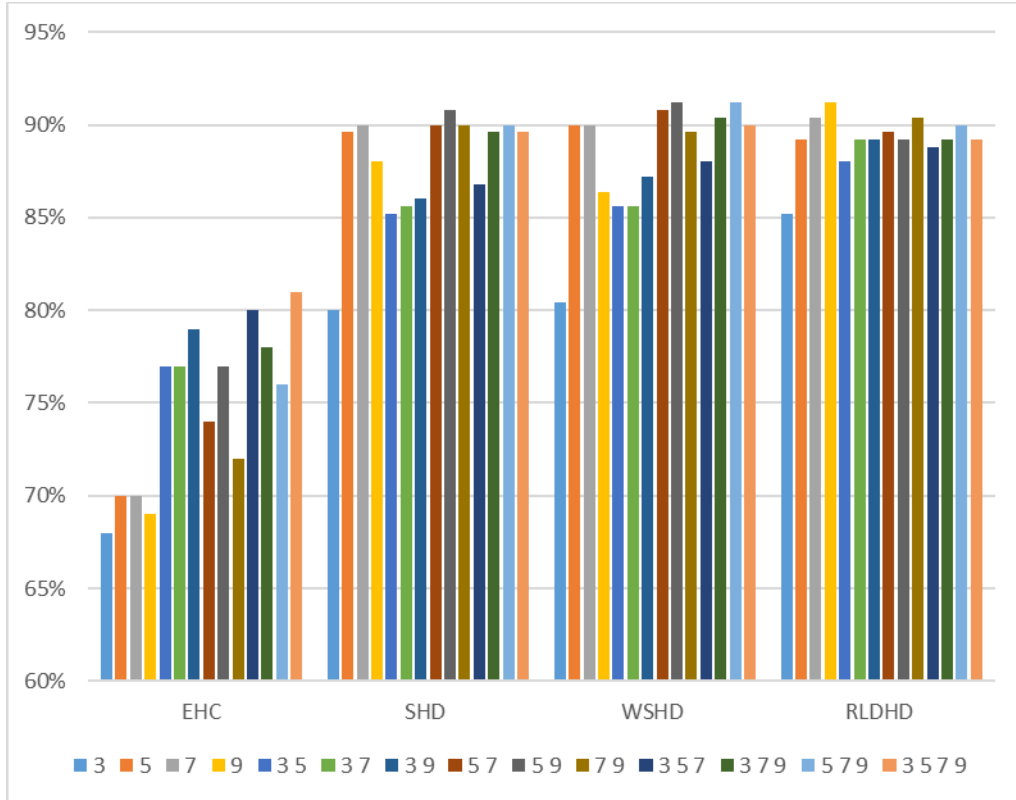


Figure 64. EHC, SHD, WSHD, RLDHD identification accuracy on Firemaker DB

### 6.2.8 Filtering With Text Localization Method

In this section, experiments were performed with combinations of various fragment length sizes (i.e. window sizes) that were considered on the filtered pages 1 and 4 of the dataset, performed on 250 writers using Manhattan Distance. The Text Localization technique was used to clean the pages, as described in Chapter 3.2. This method is appropriate to localize only pure text using some rules and dismiss all the noise produced by the writer. For comparison with previous methods, we included the results of Skeleton Hinge Distribution (SHD) as reported in [28] and Edge Skeleton Hinge Combination (ESHC) as presented previously. For consistency, the same methods were used for the filtered pages. Identification results are presented in Table 16.

Table 16. SHD, filtered SHD, ESHC and filtered ESHC identification Accuracy (Percentage) with Manhattan Distance

Fragment Length Combinations	SHD Accuracy (Percentage)	Filtered SHD Accuracy (Percentage)	ESHC Accuracy (Percentage)	Filtered ESHC Accuracy (Percentage)
3	80%	80%	79.4%	83.2%
5	89.6%	88.8%	89.2%	90%
7	90%	90%	89.6%	90.4%
9	88%	88%	87.2%	89.2%
3, 5	85.2%	85.2%	84.6%	86%
3, 7	85.6%	87.2%	85.2%	88%



3, 9	86%	86%	85.6%	88.8%
5, 7	90%	90.4%	89.6%	90%
5, 9	<b>90.8%</b>	<b>91.2%</b>	<b>90.2%</b>	90.4%
7, 9	90%	90.8%	89.4%	<b>90.8%</b>
3, 5, 7	86.8%	86.8%	86.8%	87.6%
3, 7, 9	89.6%	89.2%	89.2%	90%
5, 7, 9	90%	90.4%	89.4%	90.4%
3, 5, 7, 9	89.6%	89.6%	89.2%	89.6%

## 6.2.9 ICDAR 2017 Experiments

All the techniques were considered for testing for the ICDAR 2017 Dataset and parameters of various fragment length sizes (i.e. window sizes) combinations. Furthermore, the Quantised Skeleton Hinge Distribution was tested only by quantizing the intensity on three levels (3QSHD) since this level achieved the best accuracy on the Firemaker dataset. From the Top 1 identification results presented in Table 17, it is easily observable that SHD, WSHD and SRLDSHD have no significant differences. Furthermore, RLDSHD, although for most fragment length combinations, performs slightly worse than the other 2, for single fragment lengths like 3, 5, 7 and 9, performs slightly better. The RLDHD performs worse than SHD, with an average of 3.61% lower than the other three techniques and in all fragment length combinations besides the single fragment length 9, where an increase of 0.64% from the SHD technique can be observed. The QSHD technique had a significantly lower accuracy with an average of 10.59% lower than the SHD technique.

Table 17. SHD, WSHD, RLDSHD, RLDHD, SRLDSHD TOP-1 Identification Accuracy (Percentage) on ICDAR 2017 writer identification competition Data Set

Fragment Length Combinations	SHD Accuracy (Percentage)	WSHD Accuracy (Percentage)	RLDSHD Accuracy (Percentage)	RLDHD Accuracy (Percentage)	3QSHD Accuracy (Percentage)
3	60.83%	60.75%	64.05%	58.91%	51.91%
5	66%	65.94%	66.55%	62.22%	55.77%
7	64.63%	64.61%	65.30%	62.72%	53.63%
9	61.41%	61.41%	62.44%	62.05%	49.33%
3, 5	65.58%	65.55%	65.80%	61%	55.77%
3, 7	67.33%	67.25%	66.27%	62.19%	57.5%
3, 9	67.52%	67.52%	65.88%	63.16%	56.36%
5, 7	67.22%	67.22%	66.55%	63%	57.33%
5, 9	67.66%	67.63%	66.19%	63.61%	56.38%
7, 9	64.33%	64.33%	64.19%	62.80%	52.86%
3, 5, 7	67.75%	67.69%	66.41%	62.30%	57.66%
3, 7, 9	68.36%	67.80%	66.05%	63.38%	57.05%
5, 7, 9	67.33%	67.38%	66.05%	63.19%	56.58%
3, 5, 7, 9	<b>68.44%</b>	68.41%	66.44%	63.30%	57.94%

From the MAP identification results presented in Table 18, the same observations can be made. It is easily observable that SHD, WSHD and RLDSHD have no significant differences while RLDSHD, although for most fragment length combinations, performs slightly worse than the other 2. Single fragment lengths like 3 and 9 perform slightly better. The SRLDHD performs worse than SHD, with an average of 3.87% lower than the other three techniques and in all fragment length

combinations. The QSHD technique had a significantly lower accuracy with an average of 10.41% lower than the SHD technique.

Table 18. SHD, WSHD, RLDSHD, RLDHD, 3QSHD MAP Identification Accuracy (Percentage) on ICDAR 2017 writer identification competition Data Set

Fragment Length Combinations	SHD Accuracy (Percentage)	WSHD Accuracy (Percentage)	RLDSHD Accuracy (Percentage)	RLDHD Accuracy (Percentage)	3QSHD Accuracy (Percentage)
3	40.57%	40.48%	42.79%	38.82%	31.77%
5	44.80%	44.77%	44.26%	40.84%	34.83%
7	43.96%	43.96%	43.60%	41.37%	33.57%
9	40.99%	41%	41.71%	40.91%	30.54%
3, 5	44.50%	44.44%	44.01%	40.22%	34.78%
3, 7	46.20%	46.16%	44.32%	41.15%	35.86%
3, 9	46.33%	46.3%	44.11%	41.63%	35.28%
5, 7	45.98%	45.97%	44.29%	41.45%	35.59%
5, 9	46.34%	46.32%	43.99%	41.76%	35.35%
7, 9	43.73%	43.76%	42.94%	41.30%	33.05%
3, 5, 7	46.34%	46.30%	44.40%	41.10%	36.10%
3, 7, 9	46.92%	46.70%	44.13%	41.72%	35.83%
5, 7, 9	46.11%	46.11%	43.94%	41.64%	35.32%
3, 5, 7, 9	<b>47.02%</b>	47%	44.32%	41.65%	36.25%

Finally, in Table 19, an overview of the maximum accuracy achieved for all four techniques and results reported in the ICDAR 2017 writer identification competition is presented for the MAP and Top -1 metrics. It is noticeable that there is a lot of room for improvement for both metrics. For the MAP metric, most techniques score below 50% accuracy, while Groningen and Tebessa 2 methods achieve 54.2% and 55.6%. For the top-1 Metric, most techniques are scoring below 70%, while Groningen and Tebessa 2 methods achieve 76.1% and 76.4%, respectively.

Table 19. Skeleton Hinge Distribution Accuracy (Percentage) on ICDAR 2017 writer identification competition Data Set as reported in [21]

Method	MAP	Top-1 precision
Skeleton Hinge	47%	68.4%
WSHD	47%	68.4%
SRLDSHD	44.4%	66.5%
SRLDHD	41.7%	63.6%
3QSHD	36.2%	57.9%
Barcelona	45.9%	67%
Fribourg	30.7%	47.8%
Groningen	54.2%	76.1%
Hamburg	46.9%	67.1%
Tebessa I	52.5%	74.4%
Tebessa II	55.6%	76.4%

## 7. Discussions And Conclusion

### 7.1 Directional Hinge Features Interpretation

In this section, an attempt is made to explain and interpret the characteristics of handwritten text captured by the Directional Hinge methods described above. The common denominator of all Directional methods described in previous chapters is that they use a probability distribution  $P(\phi_1, \phi_2)$  which captures information about the Slant and the curvature of the handwritten text.

Slant is a salient feature of western handwriting [97] and is defined as the predominant angle of the downward stroke. Slanted characters can slope either to the left or right, although the Slant is not always uniform and can change even in the same word. For an example, see Figures 65 and 66.

The importance of Slant on the task of Writer Identification systems can be seen in the various works found in the literature like [24], [41], [98], [99]. Furthermore, Forensic document examiners also find Slant to be a significant consideration [100] and a discriminatory characteristic [101] to identify the writer. Again, Slant is among the most visible attributes of handwritten text, along with size and spaces. Moreover, imitating the writing Slant is one of the most common characteristics in forgery, i.e. when a writer tries to mimic other writers handwriting. According to [102], while copying Slant, the forger might lose attention for a moment and revert to his unique style. For a forensic document examiner, this sudden and brief Slant change is suspicious and might contain information about the forger identity.

Finally, in cases of disguise, i.e. the writer tries to hide his identity by changing his writing style, and he achieves that by changing his Slant of writing. In experiments performed in [97], they found that while Slant is very important for writer identification, it is not essential as a sole factor. The same observation can be seen in the Edge-Direction distribution [24], which mostly captures the Slant of writing by the low identification accuracy achieved on the Firemaker dataset.

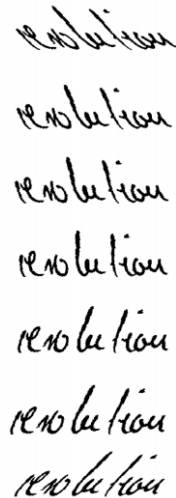


Figure 65. An example of different Slant Angles from left to right. The graphic is from [103].

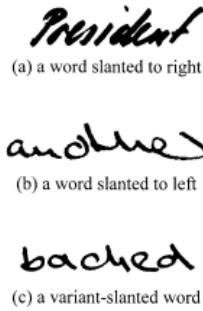


Figure 66. An example of right slanted (a), left slanted (b) and variant slanted(c) word. The graphic is from [104].

Slant angle, for most writers, is visible in the feature space when it is projected to polar coordinates. For example, in Figures 67-70, two parts of handwritten pages can be seen along with their feature space projected in polar coordinates. For the first writer, i.e. Figures 67 and 68, it is observable that the Slant of writing is precisely 90 degrees; this can be seen from the  $\phi_1$  angle distribution that maxes out at 90 degrees, while the  $\phi_2$  angle distribution maxes out at 270 degrees. Thus, by following the peaks of  $\phi_2$  towards  $\phi_1$ , the slant angle of writing is found. On the second writer, i.e. Figures 69 and 70, a right slant can be observed with an angle of approximately 81 degrees. However, it should be noted that the Slant could not be found in all the cases by finding the max of the angle distributions in the polar plot. In those cases, the predominant angles captured in the Directional feature come from all kinds of strokes, not only the downward strokes.

Bob, David en sexy Kantippe sparen postzegels van de landen Egypte, Japan, Algerje, de USA, Holland, Italië, Griekenland en Canada.

Zij bezochten veilingen en reisden met de KLM. Voor korte afstanden huurden ze een auto, meestal een VW of een Ford.

Figure 67. Part of text from Firemaker DataSet from writer 1657

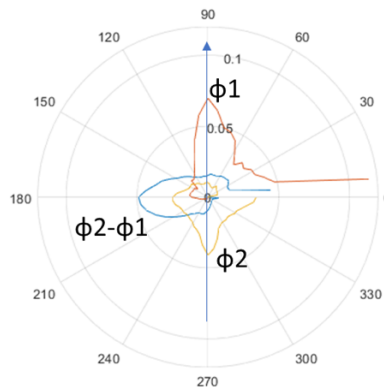


Figure 68 Polar plot of the angles  $\phi_1$ ,  $\phi_2$  and their difference  $\phi_2 - \phi_1$  for writer 1657

Bob, David en sexy kantippe sparen postzegels van de landen Egypte, Japan, Algerije, de USA, Holland, Italië, Griekenland en Canada.

Zij bezoeken veilingen en reizen met de KLM. Voor korte afstanden huurden ze een auto, meestal een VW of een Ford.

Figure 69 Part of text from Firemaker DataSet from writer 17

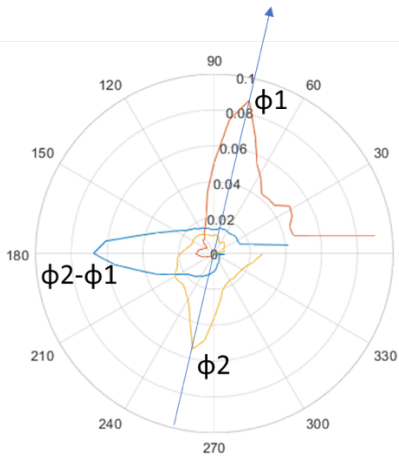


Figure 70 Polar plot of the angles  $\phi_1$ ,  $\phi_2$  and their difference  $\phi_2 - \phi_1$  for writer 17

Curvature results from the movement of the wrist and the fingers [105] while holding down a pen and in the spatial domain is expressed by the angular information of the handwritten curves [24]. Therefore, it is also an essential characteristic that plays a significant role in Writer Identification [24], [25].

The curvature information is part of the probability distribution of all the  $\phi_1$  angles and  $\phi_2$  angles and their difference ( $\phi_2 - \phi_1$ ). Although the curvature is not quite as visible as Slant in the polar plots as a feature, its importance can be realized through the experimental results presented in chapter 6. More specifically, in the identification accuracy difference between the methods of Edge Direction distribution, [24] and Edge Hinge Distribution [24].

Although Slant and Curvature are significant features for writer identification, that does not mean that they can uniquely identify the writer. It is interesting to observe the rare cases of false matching and the feature similarity between two distinct writers. In most of the miss-match cases, it is pretty interesting that the predominant direction was not relating to the Slant, i.e. downward strokes, but instead with a more horizontal direction.

in New York, Tokyo, Québec, Phoenix, Rome, Parijs,  
Zürich en Oslo.

Omdat de veilingen steeds begonnen om 12 uur  
en je gemiddeld 200 tot 300 kilometer moest  
rijden, stonden zij steeds om 6.30 uur op en

te wachten, landt er opeens een ufo. <sup>\*</sup>  
Zo zeg, wat kijkt dat beest dan, laat ik maar even  
dan terugkijken. Baf!! . zeg!! , dat is niet  
eerlijke dan waren, jij hebt een bokshandschoen

Figure 71 Train and Test samples from writer 52 of Firemaker Dataset

New York, Tokyo, Québec, Phoenix, Rome, Parijs,  
Zürich en Oslo.

Omdat de veilingen steeds begonnen om 12 uur en  
je gemiddeld 200 tot 300 kilometer moest rijden,  
stonden zij ~~reeds~~ steeds om 6.30 uur op en vertrokken  
om 8 uur uit het hotel.

Het weren met de drie ogen komt naar Henk toe  
en slaat hem op zijn neus.  
Henk heeft veel pijn en blijft zitten op de grond  
Het weren gaat weer in zijn schip zitten, zijn  
opdracht zit erop. Henk snapt er niets

Figure 72 Train and Test samples from writer 23 of Firemaker Dataset

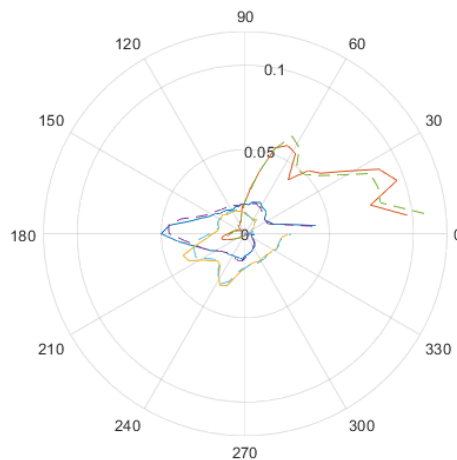


Figure 73 with solid lines writer 52 from train dataset and dashed line writer 23 from the test dataset.

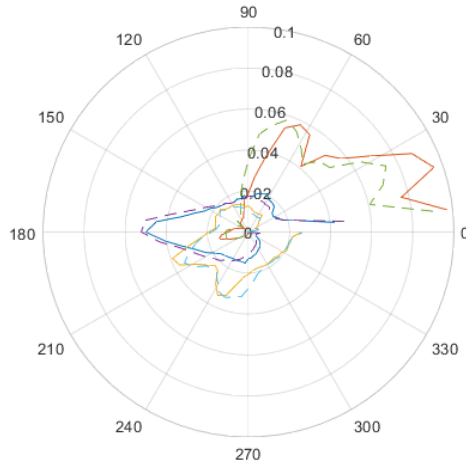


Figure 74 writer 52 differences between train and test dataset

Bob	Bob
gulden	gulden
Canada	Canada
Tokyo,	Tokyo.
begonnen	begonnen
gemiddeld	gemiddeld

Figure 75 Same words from writer 52 and 23 from Firemaker data set

Although it might be an easy task for a forensic document examiner to distinguish between the two writers in Figures 71 and 72, Directional Distribution systems have difficulty doing so. Observing the extracted angular information between those writers in Figures 73 and 74, it is apparent that the features of the two writers have more similarities than the features of the same writer between the test and training set. Furthermore, a selection of words was made to showcase the similarities of the two writers in Figure 75.

## 7.2 Discussions

Offline Writer Identification is an exciting but also a very challenging task. It has applications in sensitive fields like forensics [10], biometrics [2] and palaeography [1], and thus the mechanisms and techniques that are utilized to provide writer identification results should comply with some essential characteristics. To be more precise, Writer Identifications systems should be easy to explain, understand, and, most importantly, trust. Implications of false positives or wrong identification results in Writer Identification could have severe consequences. For example, a wrong identification used in a court case could lead to an unjust ruling. Likewise, used in a biometric system could result in a data breach, while in

palaeography, it could lead to wrong conclusions or, even worse, to future conflicts if it is about a biblical text like the Quran or the bible.

Classical Methods like Hinge distribution have an advantage over Artificial Intelligence systems, primarily for their ability to be explained. Usually, Classical methods consist of algorithms with a bounded set of steps that use other algorithms as building blocks. On the other hand, Artificial Intelligence methods feed test and train data, usually on a neural network that can adjust inner weights between neurons and learn to identify the writer based on the data provided.

Artificial intelligence methods have recently bloomed in the field of Writer Identification, outperforming traditional methods [20]. In addition, modern AI tools and frameworks and hardware advances have boosted Artificial Intelligence presence in literature publications, making Classical methods rarer.

We believe that the research trend in Artificial Intelligence will grow even more in the future. However, eventually, we might reach a point where Artificial Intelligence will produce new classical methods for Writer Identification, i.e. explainable algorithms produced by AI. Alternatively, we will revert to classical methods for the kinds of applications that require trustability and explainability.

### 7.3 Conclusion

In this work, several features for writer identification were presented. Our experiments indicate that even by using a single feature, writer identification accuracy yields promising results. While most of our experiments that achieved maximum accuracy are performed using nearest neighbour matching, other matching techniques were considered, including machine learning, yielding promising results.

One of our main findings is the importance of the skeleton information on Writer Identification methods. Our primary assumption that all stroke widths, i.e. line thickness, should be considered the same size, has been explored by applying skeletonization to characters and thus making all strokes having the same line thickness. However, the experimental results proved that the previous assumption is correct.

Furthermore, a devised technique, the Run Length Directional Hinge Distribution, considers the complete information found on the document. The same technique was limited to only using the image's Skeleton as starting points in the Run Length Directional Skeleton Hinge Distribution. Experiments on ICDAR 2017 data set revealed that when using the Skeleton, an increase in accuracy could be observed with a mean difference of 3.17%. Although the difference is not significant, it proves that better quality and fewer noise feature vectors are acquired when using the Skeleton. Furthermore, when RLDHD is compared with the Skeleton Hinge Distribution technique, the same observation can be made with a slightly higher mean difference of 3.61%.

Moreover, an attempt was made to understand the effect of Main Body Size fluctuations, observed on the document level, on identification accuracy. A Weighted variation of the Skeleton Hinge Distribution method was utilized on two datasets. Experimental results revealed that Main Body Size fluctuations hardly affect the identification accuracy since only minor differences could be observed, and thus, our assumption that Main Body size can affect writer identification is proved wrong.

Finally, an attempt was made to understand the effects of Grey-scale pixel intensity on identification accuracy. A variation of the Skeleton Hinge Distribution technique considers only pixels in a specific pixel intensity range. In this method, an attempt was made to denote pixel



intensity as the pressure of writing and prove that areas with more pressure contain more information about the writer. For the Firemaker dataset, a slight improvement in accuracy of 1.6% can be observed. On the other hand, for the ICDAR 2017 data set, a significant decline with a mean difference of 10.59 % can be observed. However, this difference might be caused by differences in datasets since Firemaker contains grey-scale samples in white background and with higher variation in the dark pixel intensities. In comparison, the ICDAR 2017 datasets contain colour images with a yellowish background and more minor variations in pixel intensities of the dark pixels that contain text. Therefore, we estimate that further research is required in more datasets with a higher variation in dark pixel intensities to prove or disprove our third assumption. We strongly believe that further improvements can be achieved. A combination of statistical features along with the skeleton hinge distribution could be used to increase accuracy. Further research is needed in the area.

Furthermore, the methods described in this work can be used for a variety of different applications. Some suggestions of possible future applications are presented here.

First of all, the techniques presented here could be used as a screening method to reduce the number of possible writers of a handwritten document image by displaying the nearest N writers. Especially when the number of writers is vast, the time needed to calculate the distances between writers is very fast since a single mathematical operation is needed per writer. Next, depending on the application, a human expert or an Artificial Intelligence method could do one on one matching. Skeleton hinge distribution features can also be used as a writer verification system by applying a threshold. For example, if the distance between the two samples is lower than a predefined threshold, then verification of the writer can be made.

In the same way, it can be used as a user authentication method or as an addition to two-factor authentication for mobile phones. Online features can be added as well to improve results.

Furthermore, it can be used for historical documents of unknown origin. There exist numerous documents, that their origin till today is unknown. With our proposed methods, a match of these documents and their writers can be made, which might give a better perspective on history.

Lastly, the skeleton hinge distribution feature suggested in this work might be a fit for other applications. For example, it is believed that it can be advantageous in slant correction systems. It might have applications in word spotting systems, but further research is needed to determine that.

## References

- [1] M. Popović, M. A. Dhali, and L. Schomaker, “Artificial intelligence based writer identification generates new evidence for the unknown scribes of the Dead Sea Scrolls exemplified by the Great Isaiah Scroll (1QIsaa),” *PloS one*, vol. 16, no. 4, p. e0249769, 2021.
- [2] C. Vielhauer, *Biometric user authentication for IT security: from fundamentals to handwriting*, vol. 18. Springer Science & Business Media, 2005.
- [3] A. K. Jain, R. Bolle, and S. Pankanti, *Biometrics: personal identification in networked society*, vol. 479. Springer Science & Business Media, 2006.
- [4] A. Jain, L. Hong, and S. Pankanti, “Biometric identification,” *Communications of the ACM*, vol. 43, no. 2, pp. 90–98, 2000.
- [5] J. Bigun and F. Smeraldi, *Audio-and Video-Based Biometric Person Authentication: Third International Conference, AVBPA 2001 Halmstad, Sweden, June 6-8, 2001. Proceedings*, vol. 2091. Springer, 2003.
- [6] R. Plamondon and G. Lorette, “Automatic signature verification and writer identification—the state of the art,” *Pattern recognition*, vol. 22, no. 2, pp. 107–131, 1989.
- [7] A. Bensefia, A. Nosary, T. Paquet, and L. Heutte, “Writer identification by writer’s invariants,” in *Proceedings Eighth International Workshop on Frontiers in Handwriting Recognition*, 2002, pp. 274–279.
- [8] A. Séropian, “Analyse de document et identification de scripteurs,” *Doctorat de l’université de Toulon et du Var, France*, vol. 18, 2003.
- [9] M. Philipp, “Fakten zu fish, das forensische informations-system handschriften des bundeskriminalamtes-eine analyse nach über 5 jahren wirkbetrieb,” 1996.
- [10] L. Schomaker, “Advances in writer identification and verification,” in *Ninth International Conference on Document Analysis and Recognition (ICDAR 2007)*, 2007, vol. 2, pp. 1268–1273.
- [11] A. Nosary, L. Heutte, T. Paquet, and Y. Lecourtier, “Defining writer’s invariants to adapt the recognition task,” in *Proceedings of the Fifth International Conference on Document Analysis and Recognition. ICDAR’99 (Cat. No. PR00318)*, 1999, pp. 765–768.
- [12] H. E. S. Said, T. N. Tan, and K. D. Baker, “Personal identification based on handwriting,” *Pattern Recognition*, vol. 33, no. 1, pp. 149–160, 2000.
- [13] U.-V. Marti, R. Messerli, and H. Bunke, “Writer identification using text line based features,” in *Proceedings of Sixth International Conference on Document Analysis and Recognition*, 2001, pp. 101–105.
- [14] L. Schomaker and L. Vuurpijl, “Forensic writer identification: a benchmark data set and a comparison of two systems (internal report for the Netherlands Forensic Institute).” Nijmegen, 2000.
- [15] S. Fiel *et al.*, “Icdar2017 competition on historical document writer identification (historical-wi),” in *2017 14th IAPR International Conference on Document Analysis and Recognition (ICDAR)*, 2017, vol. 1, pp. 1377–1382.
- [16] S. Fiel and R. Sablatnig, “Writer identification and retrieval using a convolutional neural network,” in *International Conference on Computer Analysis of Images and Patterns*, 2015, pp. 26–37.

- [17] A. Rehman, S. Naz, and M. I. Razzak, "Writer identification using machine learning approaches: a comprehensive review," *Multimedia Tools and Applications*, vol. 78, no. 8, pp. 10889–10931, 2019.
- [18] S. He and L. Schomaker, "Deep adaptive learning for writer identification based on single handwritten word images," *Pattern Recognition*, vol. 88, pp. 64–74, 2019.
- [19] S. He and L. Schomaker, "Fragnet: Writer identification using deep fragment networks," *IEEE Transactions on Information Forensics and Security*, vol. 15, pp. 3013–3022, 2020.
- [20] S. He and L. Schomaker, "GR-RNN: Global-context residual recurrent neural networks for writer identification," *Pattern Recognition*, vol. 117, p. 107975, 2021.
- [21] Y. Tang and X. Wu, "Text-independent writer identification via CNN features and joint Bayesian," in *2016 15th International Conference on Frontiers in Handwriting Recognition (ICFHR)*, 2016, pp. 566–571.
- [22] E. Commission, "Europe fit for the Digital Age: Artificial Intelligence." [Online]. Available: [https://ec.europa.eu/commission/presscorner/detail/en/ip\\_21\\_1682](https://ec.europa.eu/commission/presscorner/detail/en/ip_21_1682)
- [23] L. Schomaker, "Dilemmas in the application of artificial intelligence methods in digital paleography." Accessed: Jul. 03, 2021. [Online]. Available: <https://www.youtube.com/watch?v=chVdYOBnOuw>
- [24] M. Bulacu, L. Schomaker, and L. Vuurpijl, "Writer identification using edge-based directional features," *writer*, vol. 1, p. 1, 2003.
- [25] L. van der Maaten and E. O. Postma, "Improving automatic writer identification.," in *BNAIC*, 2005, pp. 260–266.
- [26] A. A. Brink, J. Smit, M. L. Bulacu, and L. R. B. Schomaker, "Writer identification using directional ink-trace width measurements," *Pattern Recognition*, vol. 45, no. 1, pp. 162–171, 2012.
- [27] S. He and L. Schomaker, "Co-occurrence features for writer identification," in *2016 15th International Conference on Frontiers in Handwriting Recognition (ICFHR)*, 2016, pp. 78–83.
- [28] P. Diamantatos, E. Kavallieratou, and S. Gritzalis, "Skeleton Hinge Distribution for Writer Identification," *International Journal on Artificial Intelligence Tools*, vol. 25, no. 03, p. 1650015, 2016.
- [29] P. Diamantatos, V. Verras, and E. Kavallieratou, "Detecting main body size in document images," in *2013 12th International Conference on Document Analysis and Recognition*, 2013, pp. 1160–1164.
- [30] S. He, M. Wiering, and L. Schomaker, "Junction detection in handwritten documents and its application to writer identification," *Pattern Recognition*, vol. 48, no. 12, pp. 4036–4048, 2015.
- [31] E. N. Zois and V. Anastassopoulos, "Morphological waveform coding for writer identification," *Pattern Recognition*, vol. 33, no. 3, pp. 385–398, 2000.
- [32] S. N. Srihari, M. J. Beal, K. Bandi, V. Shah, and P. Krishnamurthy, "A statistical model for writer verification," in *Eighth International Conference on Document Analysis and Recognition (ICDAR'05)*, 2005, pp. 1105–1109.
- [33] A. Bensefia, T. Paquet, and L. Heutte, "Handwritten document analysis for automatic writer recognition," *ELCVIA: electronic letters on computer vision and image analysis*, pp. 72–86, 2005.

- [34] L. Schomaker, M. Bulacu, and K. Franke, "Automatic writer identification using fragmented connected-component contours," in *Ninth International Workshop on Frontiers in Handwriting Recognition*, 2004, pp. 185–190.
- [35] A. Schlappbach and H. Bunke, "A writer identification and verification system using HMM based recognizers," *Pattern analysis and applications*, vol. 10, no. 1, pp. 33–43, 2007.
- [36] V. Pervouchine and G. Leedham, "Extraction and analysis of forensic document examiner features used for writer identification," *Pattern Recognition*, vol. 40, no. 3, pp. 1004–1013, 2007.
- [37] I. Bar-Yosef, I. Beckman, K. Kedem, and I. Dinstein, "Binarization, character extraction, and writer identification of historical Hebrew calligraphy documents," *International Journal of Document Analysis and Recognition (IJDAR)*, vol. 9, no. 2–4, pp. 89–99, 2007.
- [38] B. Li, Z. Sun, and T. Tan, "Hierarchical shape primitive features for online text-independent writer identification," in *2009 10th International Conference on Document Analysis and Recognition*, 2009, pp. 986–990.
- [39] Z. He, X. You, and Y. Y. Tang, "Writer identification of Chinese handwriting documents using hidden Markov tree model," *Pattern Recognition*, vol. 41, no. 4, pp. 1295–1307, 2008.
- [40] Y. Yan, Q. Chen, W. Deng, and F. Yuan, "Chinese handwriting identification based on stable spectral feature of texture images," *International Journal of Intelligent Engineering and Systems*, vol. 2, no. 1, pp. 17–22, 2009.
- [41] M. Bulacu and L. Schomaker, "Text-independent writer identification and verification using textural and allographic features," *IEEE transactions on pattern analysis and machine intelligence*, vol. 29, no. 4, pp. 701–717, 2007.
- [42] A. Al-Dmour and R. Abu Zitar, "Arabic writer identification based on hybrid spectral–statistical measures," *Journal of Experimental & Theoretical Artificial Intelligence*, vol. 19, no. 4, pp. 307–332, 2007.
- [43] X. Wu, Y. Tang, and W. Bu, "Offline text-independent writer identification based on scale invariant feature transform," *IEEE Transactions on Information Forensics and Security*, vol. 9, no. 3, pp. 526–536, 2014.
- [44] A. Nicolaou, A. D. Bagdanov, M. Liwicki, and D. Karatzas, "Sparse radial sampling LBP for writer identification," in *2015 13th International Conference on Document Analysis and Recognition (ICDAR)*, 2015, pp. 716–720.
- [45] H. Mohammed, V. Mäergner, T. Konidaris, and H. S. Stiehl, "Normalised local Naive Bayes nearest-neighbour classifier for offline writer identification," in *2017 14th IAPR International Conference on Document Analysis and Recognition (ICDAR)*, 2017, vol. 1, pp. 1013–1018.
- [46] A. J. Newell and L. D. Griffin, "Writer identification using oriented basic image features and the delta encoding," *Pattern Recognition*, vol. 47, no. 6, pp. 2255–2265, 2014.
- [47] G. Abdeljalil, C. Djeddi, I. Siddiqi, and S. Al-Maadeed, "Writer identification on historical documents using oriented basic image features," in *2018 16th International Conference on Frontiers in Handwriting Recognition (ICFHR)*, 2018, pp. 369–373.
- [48] F. Nadia and H. Kamel, "Personal identification based on texture analysis of Arabic handwriting text," in *2006 2nd International Conference on Information & Communication Technologies*, 2006, vol. 1, pp. 1302–1307.
- [49] S. Gazzah and N. E. ben Amara, "Arabic handwriting texture analysis for writer identification using the DWT-lifting scheme," in *Ninth International Conference on Document Analysis and Recognition (ICDAR 2007)*, 2007, vol. 2, pp. 1133–1137.

- [50] S. Al-Ma'adeed, E. Mohammed, D. al Kassis, and F. Al-Muslih, "Writer identification using edge-based directional probability distribution features for arabic words," in *2008 IEEE/ACS International Conference on Computer Systems and Applications*, 2008, pp. 582–590.
- [51] A. Chahi, Y. Ruichek, R. Touahni, and others, "Block wise local binary count for off-line text-independent writer identification," *Expert Systems with Applications*, vol. 93, pp. 1–14, 2018.
- [52] A. Chahi, Y. Ruichek, R. Touahni, and others, "Cross multi-scale locally encoded gradient patterns for off-line text-independent writer identification," *Engineering Applications of Artificial Intelligence*, vol. 89, p. 103459, 2020.
- [53] L. Xing and Y. Qiao, "Deepwriter: A multi-stream deep CNN for text-independent writer identification," in *2016 15th International Conference on Frontiers in Handwriting Recognition (ICFHR)*, 2016, pp. 584–589.
- [54] F. A. Khan, F. Khelifi, M. A. Tahir, and A. Bouridane, "Dissimilarity Gaussian mixture models for efficient offline handwritten text-independent identification using SIFT and RootSIFT descriptors," *IEEE Transactions on Information Forensics and Security*, vol. 14, no. 2, pp. 289–303, 2018.
- [55] N. Stamatopoulos, B. Gatos, G. Louloudis, U. Pal, and A. Alaei, "ICDAR 2013 handwriting segmentation contest," in *2013 12th International Conference on Document Analysis and Recognition*, 2013, pp. 1402–1406.
- [56] N. Otsu, "A threshold selection method from gray-level histograms," *IEEE transactions on systems, man, and cybernetics*, vol. 9, no. 1, pp. 62–66, 1979.
- [57] J. Sauvola and M. Pietikäinen, "Adaptive document image binarization," *Pattern recognition*, vol. 33, no. 2, pp. 225–236, 2000.
- [58] P. Stathis, E. Kavallieratou, and N. Papamarkos, "An Evaluation Technique for Binarization Algorithms.," *J. Univers. Comput. Sci.*, vol. 14, no. 18, pp. 3011–3030, 2008.
- [59] A. Mishra, K. Alahari, and C. v Jawahar, "An MRF model for binarization of natural scene text," in *2011 International Conference on Document Analysis and Recognition*, 2011, pp. 11–16.
- [60] T. Wakahara and K. Kita, "Binarization of color character strings in scene images using k-means clustering and support vector machines," in *2011 International Conference on Document Analysis and Recognition*, 2011, pp. 274–278.
- [61] Y.-F. Pan, X. Hou, and C.-L. Liu, "Text localization in natural scene images based on conditional random field," in *2009 10th International Conference on Document Analysis and Recognition*, 2009, pp. 6–10.
- [62] L. Gomez and D. Karatzas, "Multi-script text extraction from natural scenes," in *2013 12th International Conference on Document Analysis and Recognition*, 2013, pp. 467–471.
- [63] J. Canny, "A computational approach to edge detection," *IEEE Transactions on pattern analysis and machine intelligence*, no. 6, pp. 679–698, 1986.
- [64] R. Mehrotra, K. R. Namuduri, and N. Ranganathan, "Gabor filter-based edge detection," *Pattern recognition*, vol. 25, no. 12, pp. 1479–1494, 1992.
- [65] T. Y. Zhang and C. Y. Suen, "A fast parallel algorithm for thinning digital patterns," *Communications of the ACM*, vol. 27, no. 3, pp. 236–239, 1984.
- [66] L. Vincent, "Morphological grayscale reconstruction in image analysis: applications and efficient algorithms," *IEEE transactions on image processing*, vol. 2, no. 2, pp. 176–201, 1993.

- [67] F. Chang, C.-J. Chen, and C.-J. Lu, "A linear-time component-labeling algorithm using contour tracing technique," *computer vision and image understanding*, vol. 93, no. 2, pp. 206–220, 2004.
- [68] U.-V. Marti and H. Bunke, "Using a statistical language model to improve the performance of an HMM-based cursive handwriting recognition system," in *Hidden Markov models: applications in computer vision*, World Scientific, 2001, pp. 65–90.
- [69] M. Côté, E. Lecolinet, M. Cheriet, and C. Y. Suen, "Automatic reading of cursive scripts using a reading model and perceptual concepts," *International Journal on Document Analysis and Recognition*, vol. 1, no. 1, pp. 3–17, 1998.
- [70] C. K. Cheng and M. Blumenstein, "The neural-based segmentation of cursive words using enhanced heuristics," in *Eighth International Conference on Document Analysis and Recognition (ICDAR'05)*, 2005, pp. 650–654.
- [71] H. Lee and B. Verma, "A novel multiple experts and fusion based segmentation algorithm for cursive handwriting recognition," in *2008 IEEE International Joint Conference on Neural Networks (IEEE World Congress on Computational Intelligence)*, 2008, pp. 2994–2999.
- [72] A. Vinciarelli and J. Luettin, "A new normalization technique for cursive handwritten words," *Pattern recognition letters*, vol. 22, no. 9, pp. 1043–1050, 2001.
- [73] B. Gatos, I. Pratikakis, and K. Ntirogiannis, "Segmentation based recovery of arbitrarily warped document images," in *Ninth International Conference on Document Analysis and Recognition (ICDAR 2007)*, 2007, vol. 2, pp. 989–993.
- [74] D. V. Sharma and S. Wadhwa, "Dewarping machine printed documents of gurmukhi script," in *International Conference on Information Systems for Indian Languages*, 2011, pp. 117–123.
- [75] N. Doulgeri and E. Kavallieratou, "Retrieval of historical documents by word spotting," in *Document Recognition and Retrieval XVI*, 2009, vol. 7247, p. 724706.
- [76] T. Adamek, N. E. O'Connor, and A. F. Smeaton, "Word matching using single closed contours for indexing handwritten historical documents," *International Journal of Document Analysis and Recognition (IJDAR)*, vol. 9, no. 2–4, pp. 153–165, 2007.
- [77] J. A. Rodriguez-Serrano and F. Perronnin, "Handwritten word-spotting using hidden Markov models and universal vocabularies," *Pattern Recognition*, vol. 42, no. 9, pp. 2106–2116, 2009.
- [78] N. Vasilopoulos and E. Kavallieratou, "A classification-free word-spotting system," in *Document recognition and retrieval XX*, 2013, vol. 8658, p. 86580F.
- [79] E. Kavallieratou, N. Dromazou, N. Fakotakis, and G. Kokkinakis, "An integrated system for handwritten document image processing," *International Journal of Pattern Recognition and Artificial Intelligence*, vol. 17, no. 04, pp. 617–636, 2003.
- [80] J. S. Lim, "Two-dimensional signal and image processing," *Englewood Cliffs*, 1990.
- [81] Y. Zhong, K. Karu, and A. K. Jain, "Locating text in complex color images," *Pattern recognition*, vol. 28, no. 10, pp. 1523–1535, 1995.
- [82] C. Yao, X. Bai, W. Liu, Y. Ma, and Z. Tu, "Detecting texts of arbitrary orientations in natural images," in *2012 IEEE conference on computer vision and pattern recognition*, 2012, pp. 1083–1090.
- [83] V. C. Dinh, S. S. Chun, S. Cha, H. Ryu, and S. Sull, "An efficient method for text detection in video based on stroke width similarity," in *Asian conference on computer vision*, 2007, pp. 200–209.

- [84] A. Mishra, K. Alahari, and C. v Jawahar, "Top-down and bottom-up cues for scene text recognition," in *2012 IEEE Conference on Computer Vision and Pattern Recognition*, 2012, pp. 2687–2694.
- [85] B. Epshtein, E. Ofek, and Y. Wexler, "Detecting text in natural scenes with stroke width transform," in *2010 IEEE Computer Society Conference on Computer Vision and Pattern Recognition*, 2010, pp. 2963–2970.
- [86] J. Zhang and R. Kasturi, "Character energy and link energy-based text extraction in scene images," in *Asian conference on computer vision*, 2010, pp. 308–320.
- [87] S. M. Lucas *et al.*, "ICDAR 2003 robust reading competitions: entries, results, and future directions," *International Journal of Document Analysis and Recognition (IJ DAR)*, vol. 7, no. 2–3, pp. 105–122, 2005.
- [88] S. M. Lucas, "ICDAR 2005 text locating competition results," in *Eighth international conference on document analysis and recognition (ICDAR'05)*, 2005, pp. 80–84.
- [89] A. Shahab, F. Shafait, and A. Dengel, "ICDAR 2011 robust reading competition challenge 2: Reading text in scene images," in *2011 international conference on document analysis and recognition*, 2011, pp. 1491–1496.
- [90] D. Karatzas *et al.*, "ICDAR 2013 robust reading competition," in *2013 12th International Conference on Document Analysis and Recognition*, 2013, pp. 1484–1493.
- [91] S. M. Awaida and S. A. Mahmoud, "State of the art in off-line writer identification of handwritten text and survey of writer identification of Arabic text," *Educational Research and Reviews*, vol. 7, no. 20, pp. 445–463, 2012.
- [92] R. C. Gonzalez, S. L. Eddins, and R. E. Woods, *Digital image publishing using MATLAB*. Prentice Hall, 2004.
- [93] T. Kohonen, *Self-organization and associative memory*, vol. 8. Springer Science & Business Media, 2012.
- [94] P. Diamantatos, E. Kavallieratou, and P. Gomez-Gil, "Binarization: a Tool for Text Localization," in *2014 14th International Conference on Frontiers in Handwriting Recognition*, 2014, pp. 649–654.
- [95] Unipen, "The TrigraphSlant (Img) data set." [Online]. Available: <http://www.unipen.org/trigraphslant.html>
- [96] R. CCIR, "601-2: Encoding parameters of digital television for studio," *International Consultative Committee for Radio*, 1990.
- [97] A. A. Brink, R. M. J. Niels, R. A. van Batenburg, C. E. den Heuvel, and L. R. B. Schomaker, "Towards robust writer verification by correcting unnatural slant," *Pattern Recognition Letters*, vol. 32, no. 3, pp. 449–457, 2011.
- [98] J.-P. Crettez, "A set of handwriting families: style recognition," in *Proceedings of 3rd International Conference on Document Analysis and Recognition*, 1995, vol. 1, pp. 489–494.
- [99] F. J. Maarse, *The study of handwriting movement: Peripheral models and signal processing techniques*. Lisse [etc.]: Swets & Zeitlinger, 1987.
- [100] R. A. Huber and A. M. Headrick, *Handwriting identification: facts and fundamentals*. CRC press, 1999.
- [101] H. J. J. Hardy and W. Fagel, "Methodological aspects of handwriting identification," *Journal of Forensic Document Examination*, vol. 28, pp. 125–147, 2018.
- [102] K. M. Kopenhagen, "Forensic document examination: principles and practice," 2007.

- [103] E. Kavallieratou, L. Likforman-Sulem, and N. Vasilopoulos, “Slant removal technique for historical document images,” *Journal of Imaging*, vol. 4, no. 6, p. 80, 2018.
- [104] E. Kavallieratou, N. Fakotakis, and G. Kokkinakis, “Slant estimation algorithm for OCR systems,” *Pattern Recognition*, vol. 34, no. 12, pp. 2515–2522, 2001.
- [105] L. R. B. Schomaker, A. J. W. M. Thomassen, and H.-L. Teulings, “A computational model of cursive handwriting,” in *Computer recognition and human production of handwriting*, World Scientific, 1989, pp. 153–177.